PHYSICAL REVIEW D **89,** 085008 (2014)

Effects of divergent ghost loops on the Green's functions of QCD

A. C. Aguilar,[1] D. Binosi,[2] D. Ibañez,[2] and J. Papavassiliou[3]

[1]*University of Campinas—UNICAMP, Institute of Physics "Gleb Wataghin", 13083-859 Campinas, São Paulo, Brazil*

[2]*European Centre for Theoretical Studies in Nuclear Physics and Related Areas (ECT*) and Fondazione Bruno Kessler, Villa Tambosi, Strada delle Tabarelle 286, I-38123 Villazzano, Trento, Italy*

[3]*Department of Theoretical Physics and IFIC, University of Valencia and CSIC, E-46100 Valencia, Spain*

(Received 11 December 2013; published 3 April 2014)

In the present work, we discuss certain characteristic features encoded in some of the fundamental QCD Green's functions, for which the origin can be traced back to the nonperturbative masslessness of the ghost field, in the Landau gauge. Specifically, the ghost loops that contribute to these Green's functions display infrared divergences, akin to those encountered in the perturbative treatment, in contradistinction to the gluonic loops, for which perturbative divergences are tamed by the dynamical generation of an effective gluon mass. In $d = 4$, the aforementioned divergences are logarithmic, thus causing a relatively mild impact, whereas in $d = 3$ they are linear, giving rise to enhanced effects. In the case of the gluon propagator, these effects do not interfere with its finiteness, but make its first derivative diverge at the origin, and introduce a maximum in the region of infrared momenta. The three-gluon vertex is also affected, and the induced divergent behavior is clearly exposed in certain special kinematic configurations, usually considered in lattice simulations; the sign of the corresponding divergence is unambiguously determined. The main underlying concepts are developed in the context of a simple toy model, which demonstrates clearly the interconnected nature of the various effects. The picture that emerges is subsequently corroborated by a detailed nonperturbative analysis, combining lattice results with the dynamical integral equations governing the relevant ingredients, such as the nonperturbative ghost loop and the momentum-dependent gluon mass.

DOI: 10.1103/PhysRevD.89.085008 PACS numbers: 12.38.Aw, 12.38.Lg, 14.70.Dj

I. INTRODUCTION

In recent years our understanding of the IR sector of QCD has advanced considerably, due to a detailed and systematic scrutiny of the fundamental Green's functions of the theory. In particular, high-quality lattice simulations of propagators [1–7] and vertices [8–10] have furnished new insights on the subtle underlying mechanisms and have spurred an intense parallel activity within the various nonperturbative approaches in the continuum [11–31].

At this point, the plethora of available information needs to be interpreted carefully and be used in the construction of a reliable picture of the fundamental dynamics, with increasingly stronger predictive power. To that end, in the present work, we elaborate on what appears to be a profound connection between the masslessness of the ghost, the precise form of the gluon propagator in the deep IR, and the divergences observed in certain kinematic limits of the three-gluon vertex. This particular connection is valid in the Landau gauge, both in $d = 3, 4$; however, in $d = 3$ the associated effects are considerably more enhanced, for reasons that will become clear in what follows.

As is well known by now, the infrared finiteness of the gluon propagator and the ghost dressing function, observed in a variety of (Landau gauge) lattice simulations, may be explained in a rather natural way by invoking the concept of a dynamically generated mass [32–35]. In particular, the (Euclidean) gluon propagator $\Delta(q^2)$ assumes the form $\Delta^{-1}(q^2) = q^2 J(q^2) + m^2(q^2)$, where the first term corresponds to the "kinetic term," or "wave function" contribution, while the second denotes the momentum-dependent mass function [36,37]. Within the framework of the Schwinger–Dyson equations (SDEs), both $J(q^2)$ and $m^2(q^2)$ satisfy two independent but coupled integral equations, which, at least in principle, determine their dynamical evolution.

In $d = 4$ the main observation underlying the present work may be described as follows. The fact that the ghost propagator, $D(q^2)$, remains massless, has as consequence that the contribution to $J(q^2)$ stemming from the ghost-loop diagram [(a_3) in Fig. 1] contains a pure logarithm, $\ln q^2$, which is "unprotected," in the sense that there is no mass term in its argument that could tame its divergence in the IR. This is to be contrasted with the corresponding logarithms originating from the gluonic loops [(a_1) in Fig. 1], of the type $\ln(q^2 + m^2)$, which, due to the presence of the dynamical gluon mass $m^2(q^2)$, are finite for arbitrary Euclidean momenta. Of course, the massless logarithm does not interfere with the overall finiteness of $\Delta(q^2)$, simply because it is multiplied by q^2; its presence, however, makes the first derivative of $\Delta(q^2)$ diverge at the origin. In

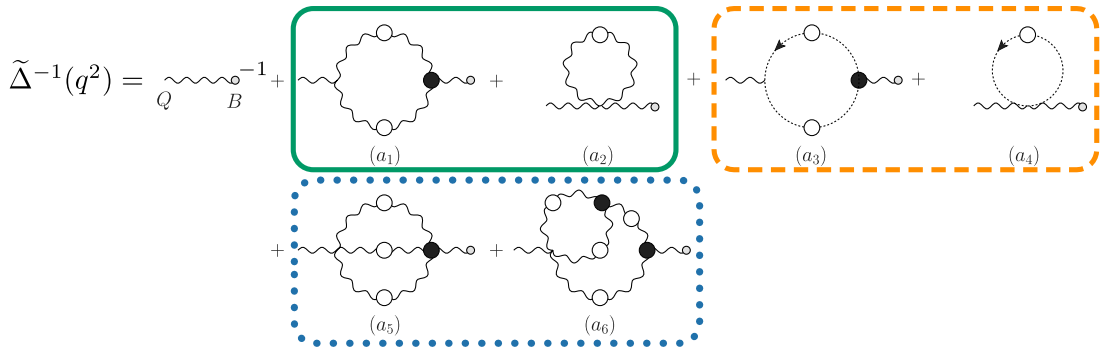

FIG. 1 (color online). The SDE obeyed by the QB gluon propagator. Each of the three different boxes (continuous, dashed, and dotted line) encloses a set of diagrams forming an individually transverse subgroup, namely, $q^\mu[(a_1)+(a_2)]_{\mu\nu}=0$, $q^\mu[(a_3)+(a_4)]_{\mu\nu}=0$, and $q^\mu[(a_5)+(a_6)]_{\mu\nu}=0$. Black (white) blobs represent fully dressed one-particle-irreducible (connected) Green's functions; finally, small gray circles appearing on the external legs indicate background gluons.

addition, it induces a subtle effect on the precise shape of the gluon propagator in the deep IR. Specifically, $\Delta(q^2)$ is not a monotonic function of q^2, displaying a (numerically small) maximum, precisely due to the $q^2\ln q^2$ term. The size and location of this effect is largely controlled by the relative weight with which the two types of logarithm contribute to $J(q^2)$; in particular, the weight of the massless logarithm is about 1 order of magnitude less than that of the massive, a fact that pushes the appearance of the effect in the deep IR, reducing at the same time its size.

It turns out that the quantity that accounts for the divergent behavior of the three-gluon vertex (for recent studies of this vertex, see also Refs. [38,39]) in some special kinematic limits studied on the lattice, is precisely the $J(q^2)$ considered above. In particular, in the "orthogonal" configuration with one momentum vanishing, the usual quantity employed in the lattice studies, to be denoted by R, satisfies $R(q^2)\sim[q^2J(q^2)]'$, where the "prime" denotes the derivative with respect to q^2. Thus, the dominant contribution as $q^2\to 0$ is $R(q^2)\sim J(q^2)\sim\ln q^2$; evidently, for sufficiently small q^2, $R(q^2)$ becomes negative and diverges as a logarithm.

In $d=3$, the situation is qualitatively similar to the one described above, but the divergences induced due to the masslessness of the ghost are stronger. Specifically, as may be already established at the level of a simple one-loop calculation [40], the part of $J(q^2)$ coming from the ghost loop behaves like $1/q$. As a result the corresponding effects are significantly enhanced: the maximum of the gluon propagator is clearly visible on the lattice [2], and so is the abrupt negative divergence seen in the corresponding $R(q^2)$ [8].

Note that our theoretical prediction for the signs of the divergence both at $d=3$, 4 is unequivocal: they are fixed by the sign of the logarithm obtained from graph (a_3) in Fig. 1 (for earlier related works, see, e.g. Refs. [41,42]). In addition, it is interesting to note that the observed divergences occur within a theory with a finite gluon propagator and a nonenhanced ghost dressing function. In fact, the origin of the divergences encountered in the three-gluon vertex is not associated in any way with the (intrinsically divergent) "scaling" solutions [17,20] but rather with the loop effects of massless (but nonenhanced) ghosts.

At this point it is useful to establish a sharp distinction between the notions of "gauge invariance" and "gauge independence." The term gauge invariance is used throughout this work for indicating that a Green's function satisfies the Ward identity (WI) or Slavnov–Taylor identity (STI), imposed by the gauge or Becchi-Rouet-Stora-Tyutin (BRST) symmetry of the theory. On the other hand, the gauge (in)dependence of a Green's function is related with the (independence of) dependence on the gauge fixing parameter (e.g., ξ) used to quantize the theory. Evidently, an off-shell Green's function may be gauge invariant but gauge dependent: for example, the QED photon-electron vertex, $\Gamma_\mu(p,p+q)$, depends explicitly on ξ but satisfies (for every value of ξ) the classic WI $q^\mu\Gamma_\mu(p,p+q)=S^{-1}(p+q)-S^{-1}(p)$. A textbook example of a Green's function that is both gauge invariant and gauge independent is the photon self-energy (vacuum polarization), which is both transverse and ξ independent. As far as the present work is concerned, it should be clear that all statements and results are particular to the Landau gauge, so they are manifestly gauge dependent. In fact, the very notion of the "ghost-loop" contributions to the gluon propagator is gauge dependent; in noncovariant gauge fixing schemes, for example, the ghost fields decouple from the gluon Green's functions.[1] So, in general, by gauge invariant we mean "STI preserving," or in the specific case of the gluon propagator, we mean the arrangement of graphs into "individually transverse" subsets.

The reader should be aware of the fact that the present analysis, as practically any other based on SDEs, suffers

[1]Notice, however, that Green's functions involving external ghost fields might be nontrivial even in such gauges; for example in the Coulomb gauge, the ghost propagator has been simulated on the lattice, see *e.g.*, [43] and references therein.

from the perennial limitations inherent to this particular formalism, namely, the lack of an expansion parameter, or a rigorous criterion for estimating the truncation errors. What we have tried to accomplish throughout this work is to truncate in a way that maintains the gauge symmetry intact, in an attempt to minimize the contamination of the results from gauge artifacts. However, the nonlinear propagation of effects originating from the (omitted) higher-order Green's functions cannot be *a priori* discarded, and their possible numerical impact may not be reliably estimated; instead, they may be only *a posteriori* determined, e.g., through the detailed comparison of the SDE results with those obtained through systematic nonperturbative methods, such as the lattice.

The article is organized as follows. In Sec. II we present a simple description of the gluon propagator, which captures quite faithfully all qualitative features mentioned above. This section serves as a reference for fixing the main ideas and can guide the reader through the more complex analysis that follows. In Sec. III we venture into the full nonperturbative analysis of the divergent ghost loop and the implication for the gluon propagator and the three-gluon vertex. Throughout this study we make extensive use of the full nonperturbative equation governing the momentum evolution of the gluon mass, derived in Ref. [37]. Finally, in Sec. IV we discuss our main results and present our conclusions. The article ends with four Appendices. In Appendix A we discuss the R projector in a technically simplified but qualitatively accurate setting. In Appendix B the subleading nature of the transverse part of the ghost-gluon vertex is established. In Appendix C we discuss the background field method (BFM) Green's functions as an alternative for resolving the peak structure of the gluon propagator. Finally, in Appendix D we present a brief discussion of the scaling solutions and contrast their main features to the massive scenario considered here.

II. MASSIVE VS MASSLESS LOOPS: A QUALITATIVE DESCRIPTION

In this section we discuss the general ideas that underly the present work and introduce a simple, one-loop inspired model, which explains, with little calculational effort, the main effects.

A. General considerations

In what follows we will work in the Landau gauge, where the full gluon propagator takes the form

$$i\Delta_{\mu\nu}(q) = -iP_{\mu\nu}(q)\Delta(q^2); \qquad P_{\mu\nu}(q) = g_{\mu\nu} - q_\mu q_\nu/q^2. \tag{2.1}$$

In addition, the ghost propagator $D(q^2)$ and its dressing function, $F(q^2)$, are related by

$$D(q^2) = \frac{F(q^2)}{q^2}. \tag{2.2}$$

We will now consider the SDE obtained through the combination of the pinch technique (PT) [32,44–47] with the BFM [48], known as the PT-BFM scheme [23,24,49]. Specifically, the SDE for the conventional gluon propagator reads

$$\Delta^{-1}(q^2)P_{\mu\nu}(q) = \frac{q^2 P_{\mu\nu}(q) + i\sum_{i=1}^{6}(a_i)_{\mu\nu}}{1+G(q^2)}, \tag{2.3}$$

where the diagrams (a_i) are shown in Fig. 1. Note that these diagrams give rise to the self-energy of $\tilde{\Delta}(q^2)$, namely, the propagator formed by a quantum gluon (Q) and a background one (B). Thus, Eq. (2.3) is the nonperturbative diagrammatic representation of the formal relation

$$[1+G(q^2)]\Delta^{-1}(q^2) = \tilde{\Delta}^{-1}(q^2), \tag{2.4}$$

known in the literature [50,51] as a background-quantum identity (BQI). A SDE similar to that of Eq. (2.3), but with more diagrams, relates $\Delta(q^2)$ with the propagator $\hat{\Delta}(q^2)$, formed by two background gluons (B^2) [49]; the corresponding BQI reads

$$[1+G(q^2)]^2\Delta^{-1}(q^2) = \hat{\Delta}^{-1}(q^2). \tag{2.5}$$

The auxiliary function $G(q^2)$ has been studied in detail in Ref. [52]; here it should suffice to mention that, for practical purposes, throughout the present work, we will use the approximate relation

$$1+G(q^2) \approx F^{-1}(q^2), \tag{2.6}$$

which becomes exact in the deep IR, in $d = 3, 4$, [52–55].

As was already mentioned in the introduction, in the case of an IR finite gluon propagator, the scalar function $\Delta(q^2)$ can be decomposed as (Euclidean space)

$$\Delta^{-1}(q^2) = q^2 J(q^2) + m^2(q^2), \tag{2.7}$$

where $J(q^2)$ is the inverse of the gluon dressing function and $m^2(q^2)$ is the dynamically generated (momentum-dependent) gluon mass, with the characteristic property that $m^2(0) > 0$. We emphasize that the above decomposition is not mathematically unique, in contradistinction to the case of the quark self-energy, where the corresponding separation is realized unambiguously, due to the distinct Dirac properties of the two quantities appearing in it, namely, a Dirac vector (quark wave function) and a Dirac scalar (quark mass). The main guiding principle in implementing this separation at the level of the gluon SDE has been explained in detail in Refs. [36,37].

Note that Eq. (2.4) is satisfied separately by the kinetic and the mass terms [36]; thus, using the approximation (2.6), we have

$$J(q^2) = F(q^2)\tilde{J}(q^2); \qquad m^2(q^2) = F(q^2)\tilde{m}^2(q^2). \quad (2.8)$$

A completely analogous relation, obtained from Eq. (2.5), relates $J(q^2)$ with $\hat{J}(q^2)$ [see Eq. (A3)], as well as the corresponding gluon masses.

Given that the function $F(q^2)$ has been simulated accurately on the lattice, Eq. (2.8) allows one to obtain $J(q^2)$ from $\tilde{J}(q^2)$; the latter is easier to calculate, due to the special properties of its diagrammatic expansion, implemented by the PT-BFM Feynman rules. In particular, since all subsets of graphs enclosed within each box Fig. 1 give rise to a transverse contribution [24,49], their individual treatment (or the total omission of the "two-loop dressed" subset) does not compromise the transversality of the gluon self-energy.

Even though the dynamical equation governing $\tilde{J}(q^2)$ [or, equivalently, $J(q^2)$] is not fully known, mainly due to the poor knowledge of the four-gluon vertex appearing in the two-loop dressed diagram of (a_5), the main effect that we want to study here originates from the two sets of "one-loop" dressed graphs, namely, $(a_1) + (a_2)$ and $(a_3) + (a_4)$.

It turns out that there is a profound qualitative difference between these two sets of graphs, which manifests itself in the behavior of the resulting $J(q^2)$. Specifically, the corresponding contributions to $J(q^2)$ reflect the fact that the virtual particles forming these loops (gluons and ghosts, respectively) have completely different behavior in the IR: while the gluons are effectively massive, the ghosts behave as massless particles, $D(q^2) \sim 1/q^2$. As a result, in $d = 4$, whereas the perturbative logarithm emerging from the first set of graphs is tamed by the presence of the gluon mass, and is therefore finite for all momenta, the corresponding logarithm coming from the ghost loop remains massless, and, as a consequence, it vanishes at a finite value of q^2, then reverses its sign, becoming finally divergent at $q^2 = 0$. A similar situation occurs in the $d = 3$ case, but the corresponding divergences are linear in q instead of logarithmic.

B. Toy model

The picture described above may be concisely captured by setting

$$J_{a_1}(q^2) \sim \begin{cases} \ln[(q^2+m^2)/\mu^2], & d=4; \\ (1/q)\arctan(q/2m), & d=3, \end{cases} \quad (2.9)$$

and

$$J_{a_3}(q^2) \sim \begin{cases} \ln(q^2/\mu^2), & d=4; \\ 1/q, & d=3. \end{cases} \quad (2.10)$$

The corresponding gluon propagator then becomes

$$\Delta^{-1}(q^2) = q^2 J(q^2) + m^2 = q^2[1 + c_1 J_{a_1}(q^2) + c_3 J_{a_3}(q^2)] + m^2, \quad (2.11)$$

with c_1 and c_3 two real constants, for which the values will be fixed according to arguments given below.

In the case of $d = 4$, the form proposed for $J_{a_3}(q^2)$ corresponds simply to the one-loop integral $\int \frac{1}{k^2(k+q)^2}$, reflecting the fact that the internal ghost propagators are massless. On the other hand, $J_{a_1}(q^2)$ simulates an integral for which the internal propagators are massive.[2] As a result, the subset of logarithmic contributions originating from gluon loops [practically (a_1) in Fig. 1] undergoes the replacement[3] $\ln(q^2/\mu^2) \to \ln[(q^2+m^2)/\mu^2]$. The presence of the mass prevents this logarithm from diverging; depending on the ratio m/μ, the logarithm may turn negative past a certain value of q^2 but remains finite, reaching the final value $\ln(m^2/\mu^2)$.

On the other hand, in the $d = 3$ case, the corresponding transition from massless to massive loops is implemented through the substitution (Minkowski space)

$$\int_k \frac{1}{k^2(k+q)^2} = \left(\frac{i}{8}\right)\frac{1}{q} \longrightarrow \int_k \frac{1}{(k^2-m^2)[(k+q)^2-m^2]} = \left(\frac{i}{4\pi}\right)\frac{1}{q}\arctan\left(\frac{q}{2m}\right). \quad (2.12)$$

Returning to the values of c_1 and c_3, let us first focus on the $d = 4$ case. Given that the proposed toy model is clearly one-loop inspired, it is natural to expect that the values of c_1 and c_3 would be determined by the prefactors multiplying the corresponding one-loop diagrams. Specifically, one has

$$c_1 = 2\left(\frac{\alpha C_A}{4\pi}\right); \qquad c_3 = \frac{1}{6}\left(\frac{\alpha C_A}{4\pi}\right), \quad (2.13)$$

where C_A is the Casimir eigenvalue in the adjoint representation [$C_A = N$ for SU(N)], and $\alpha_s = g^2/4\pi$. Note that $c_1 + c_3 = \frac{13}{6}(\frac{\alpha C_A}{4\pi})$, which is precisely the total coefficient appearing in the well-known one-loop result [56], $\Delta^{-1}(q^2) = 1 + \frac{13}{6}q^2(\frac{\alpha C_A}{4\pi})\ln(q^2/\mu^2)$. In obtaining these values, we have used the asymptotic (ultraviolet) one-loop result $F(q^2) = 1 - \frac{3}{4}(\frac{\alpha C_A}{4\pi})\ln(q^2/\mu^2)$ and have replaced the perturbative logarithm by a massive one, since, as

[2]We hasten to emphasize that we do not advocate the use of naive massive gluons inside loops as a self-consistent theoretical option. In fact, such an approach would clash with a number of field-theoretic principles that the PT-BFM formalism is designed to preserve, such as the transversality of the gluon self-energy.

[3]A loop with hard masses gives rise to the textbook integral $\int_0^1 dx \ln$; however, the resulting expression does not provide any further insights to the question at hand than the simple massive logarithm employed here.

mentioned already, nonperturbatively the function $F(q^2)$ saturates at a finite value.

The corresponding values for c_1 and c_3 in $d=3$ may be determined following a completely analogous procedure, using certain auxiliary results presented in Ref. [40]; they are given by

$$c_1 = -\left(\frac{25g^2C_A}{32\pi}\right); \qquad c_3 = -\left(\frac{g^2C_A}{32}\right) \tag{2.14}$$

(notice that there is no π in c_3). In addition, since in $d=3$ the gauge coupling g^2 has dimensions of mass, so do c_1 and c_3.

In the analysis that follows, we will depart from these particular values of c_1 and c_3 in order to expose better the underlying effects. The main lessons that we will retain from the one-loop discussion given above are as follows: (i) in $d=4$, both c_1 and c_3 are positive; (ii) in $d=3$, both c_1 and c_3 are negative; and (iii) in both cases, the modulus of c_3 is significantly smaller than that of c_1.

C. Main implications

The model presented above leads to important consequences for the gluon propagator and for the three-gluon vertex.

1. Maximum of the gluon propagators

The gluon propagator, $\Delta(q^2)$, of this toy model displays a maximum, both in $d=3$, 4, or, equivalently, the inverse propagator, $\Delta^{-1}(q^2)$, displays a minimum. This can be easily established by taking the first derivative of Eq. (2.11); specifically, in $d=4$ (and with m^2 constant),

$$\begin{aligned}[\Delta^{-1}(q^2)]' &= [q^2J(q^2)]' \\ &= c_3\ln(q^2/\mu^2) + \left\{1 + c_1\ln[(q^2+m^2)/\mu^2] \right. \\ &\quad \left. + \frac{c_1q^2}{q^2+m^2} + c_3\right\}. \end{aligned} \tag{2.15}$$

The quantity in curly brackets is finite, but in general of indefinite sign, due to the presence of the logarithm. However, it is clear that for $q^2 > \mu^2$ it is positive definite, and so is the massless logarithm; in fact, for $q^2 \gg m^2$ the two logarithms combine to give the asymptotic result $\frac{13}{6}\left(\frac{\alpha C_A}{4\pi}\right)\ln(q^2/\mu^2)$. On the other hand, in the opposite momentum limit, since the first term can become arbitrarily large and negative as q^2 approaches zero (remember, $c_{1,2} > 0$), there exists a value $0 < q_\Delta^2 < \mu^2$ such that $[\Delta^{-1}(q_\Delta^2)]' = 0$, no matter how small c_3 may be; of course, as c_3 assumes smaller values, q_Δ^2 is pushed closer to zero. It is then elementary to show that the above zero of the derivative corresponds to a minimum of $\Delta^{-1}(q^2)$, since the second derivative is positive,

$$[\Delta^{-1}(q^2)]'' = \frac{c_1}{q^2+m^2} + \frac{c_1m^2}{(q^2+m^2)^2} + \frac{c_3}{q^2} > 0. \tag{2.16}$$

Thus, one reaches the conclusion that the IR divergence of the first term, caused by the masslessness of the ghost, and the positivity of the ultraviolet logarithms, reflecting the asymptotically free nature of the theory, force $\Delta(q^2)$ to have a maximum. In what follows we will denote the location of this maximum by q_Δ.

Let us emphasize that the above conditions are *sufficient* but not necessary for the existence of such a maximum. Indeed, one can easily imagine eliminating the divergent logarithm, by setting $c_3 = 0$ or saturating it (artificially) with some mass. Then, even though everything is finite in the IR, depending on the relative values of parameters and masses, one *may* still get the rhs of Eq. (2.15) to vanish. But if the massless logarithm is there, Eq. (2.15) will always have a solution.

It is of course obvious that the quantity $[q^2J(q^2)]'$ displays a minimum located exactly at the same point where the maximum of $\Delta(q^2)$ is and that the reason for this coincidence is simply the constancy of the gluon mass. However, in anticipation of the full nonperturbative analysis of the next section, where the gluon mass will be a function of q^2, we will already at this level distinguish these two points by introducing a different symbol for the location of the minimum of the kinetic term, namely, q_J. So, whereas within the toy model we have trivially $q_\Delta = q_J$, in the complete nonperturbative treatment, we will have $q_\Delta \neq q_J$.

An analogous proof may be constructed for the $d=3$ case, where the corresponding differentiation yields

$$\begin{aligned}[\Delta^{-1}(q^2)]' &= [q^2J(q^2)]' \\ &= 1 + \frac{c_1}{2q}\arctan(q/2m) + \frac{c_3}{2q} + \frac{c_1m}{q^2+4m^2}. \end{aligned} \tag{2.17}$$

To find the approximate q_Δ for which the rhs vanishes, assume that $q < m$, expand, and keep only first-order terms in q/m. Then, one arrives at the simple solution

$$q_\Delta/m = -\frac{c_3/m}{2 + c_1/m}. \tag{2.18}$$

For this solution to be consistent, we must have $0 < q_\Delta/m < 1$, or (remember that $c_{1,3} < 0$) $|c_1| + |c_3| < 2m$. This, in turn, restricts the allowed values of the (dimensionless) ratio $m/2g^2$; in particular, at the one-loop level, our toy model provides the lower bound

$$\frac{m}{2g^2} \gtrsim 0.14, \tag{2.19}$$

in agreement with a plethora of independent studies based on a variety of approaches in the continuum [57–60] and on the lattice[4] [62–65].

[4] A review on the subject of $d=3$ Yang–Mills theories can be found in Ref. [61].

2. Negative divergence of the three-gluon vertex

To understand how the (negative) IR divergences that appear in the studies of special kinematic configurations of the conventional three-gluon vertex (Q^3) are related to the properties of the $J(q^2)$, it is convenient to consider a model inspired by the PT-BFM three-gluon vertex (B^3) [44,66,67], described in detail in Appendix A. The treatment of the conventional three-gluon vertex will be addressed in the next section; it basically boils down to a technically more involved realization of the main idea presented here.

The usual quantity employed in the lattice studies of the three-gluon vertex is denoted by R ($\hat{R}$ in the B^3 case) and will be referred to as the "R projector" [for its exact definition, see Eq. (3.30)]; it receives contributions from the various form factors of the three-gluon vertex, both "longitudinal" and "transverse" (see Appendix A). Because of the QED-like WI satisfied by the B^3 vertex, as opposed to the STI satisfied by the Q^3 vertex, the former can be expressed *exclusively* in terms of the B^2 gluon kinetic term $\hat{J}(q^2)$ [with $J(q^2) = F^2(q^2)\hat{J}(q^2)$], while the latter remain undetermined (they satisfy the WI automatically). From the kinematic point of view, R depends on the modulo of two independent momenta (q^2 and r^2) and the angle φ formed between them. It turns out that for the special case $\varphi = \pi/2$ and $r^2 = 0$, any contribution from the transverse form factors of the three-gluon vertex drops out, and one finds that, quite remarkably, $\hat{R}(q^2) = [q^2\hat{J}(q^2)]'$.

It is now relatively straightforward to recognize that $\hat{J}(q^2)$ and $J(q^2)$ display the same type of logarithmic divergence in the IR, due to the masslessness of the corresponding ghost loop. Thus, even though the precise prefactors between each ghost loop do not coincide, due to the difference in the form of the ghost-gluon vertex in the linear covariant (R_ξ) gauges and in the BFM (see discussion in Sec. III), the qualitative behavior in the limit of interest is common. Furthermore, one may recover $R(q^2)$ from $\hat{R}(q^2)$ by assigning tree-level values to the ghost dressing function F and the gluon-ghost kernel H [see Eq. (3.35)]. Therefore, if we use the fact that H does not introduce additional IR divergences [see the discussion after Eq. (3.40)], then $R(q^2)$ may be qualitatively modeled by

$$R(q^2) \sim [q^2 J(q^2)]'. \tag{2.20}$$

If we now employ the toy model of the previous subsection to evaluate the rhs of Eq. (2.20), then $R(q^2)$ is given precisely by the expression obtained in Eqs. (2.15) and (2.17). Specifically, in either case,

$$R(q^2) \underset{q^2\to 0}{\sim} c_3 J_{a_3}(q^2), \tag{2.21}$$

which gives a negative logarithmic divergence in $d = 4$ [$c_3 > 0$, but $\ln(q^2/\mu^2) < 0$], and a negative linear divergence in $d = 3$ ($1/q > 0$, but $c_3 < 0$). Summarizing,

$$R(q^2) \underset{q^2\to 0}{\sim} \begin{cases} \ln(q^2/\mu^2), & d = 4; \\ -1/q, & d = 3. \end{cases} \tag{2.22}$$

Note that the value q_Δ, which determines the location of the maximum of $\Delta(q^2)$ corresponds now precisely to the "crossing point," q_0, namely, the point where R passes from positive to negative values. Thus, *within this toy model*, the location of the maximum of the gluon propagator *coincides* with the crossing point[5] of $R(q^2)$, i.e., $q_\Delta = q_0$. Of course, the reason for this coincidence is directly related to the fact that we use a constant gluon mass, m^2. If instead we had employed a momentum-dependent mass, $m^2(q^2)$, the location of these special points would differ, $q_\Delta \neq q_0$, as will happen in the full analysis of the next section.

Finally, the ultraviolet behavior of the form factor $R(q^2)$ is given by

$$R(q^2) \underset{q^2\to\infty}{\sim} \begin{cases} 1 + (c_1 + c_3)[1 + \ln(q^2/\mu^2)], & d = 4; \\ 1, & d = 3. \end{cases} \tag{2.23}$$

Thus, in the three-dimensional case $R(q^2)$ saturates at its tree-level value, while in four dimensions, it increases as a positive logarithm, $R(q^2) \to +\infty$.

3. Numerics

In Fig. 2 we plot the propagator $\Delta(q^2)$, its kinetic part $q^2J(q^2)$, and finally the quantity $R(q^2) \sim [q^2J(q^2)]'$ for some values of the c_i constants (in the four-dimensional case, we have additionally fixed[6] μ at 4.3 GeV, and, accordingly, $m^2 = 0.14$ GeV^2).

As one can see from the top panels of this figure (continuous curves), the propagator $\Delta(q^2)$ of Eq. (2.11) displays an IR peak. In $d = 3$, this particular feature is well established, both at the level of the lattice [2,68] as well as from various treatments in the continuum (see, e.g., Ref. [40]). On the other hand, in $d = 4$, the lattice evidence for the appearance of such a peak is certainly inconclusive, while in the continuum, to the best of our knowledge, this possibility has not even been contemplated. Of course, we hasten to emphasize that there are regions in the parameter space of our toy model where the "peak" flattens out completely and escapes detection due to numerical errors.

[5]If the conditions for having a maximum in the gluon propagator were not fulfilled, R would still diverge at the origin, but there would be no crossing point; R would be negative for all values of momenta.

[6]The choice $\mu = 4.3$ GeV is lattice motivated, in the sense that it corresponds to the last available point in the ultraviolet tail of the gluon propagator obtained from the simulation of Ref. [3]; therefore, in the full nonperturbative treatment, one usually renormalizes the gluon propagator such that $\Delta^{-1}(\mu^2) = \mu^2$, at that particular point. Then, the IR saturation point acquires the value $\Delta^{-1}(0) = m^2 = 0.14$ GeV^2. At the level of the toy model, these choices simply help us maintain a close analogy with the full treatment presented in the next section.

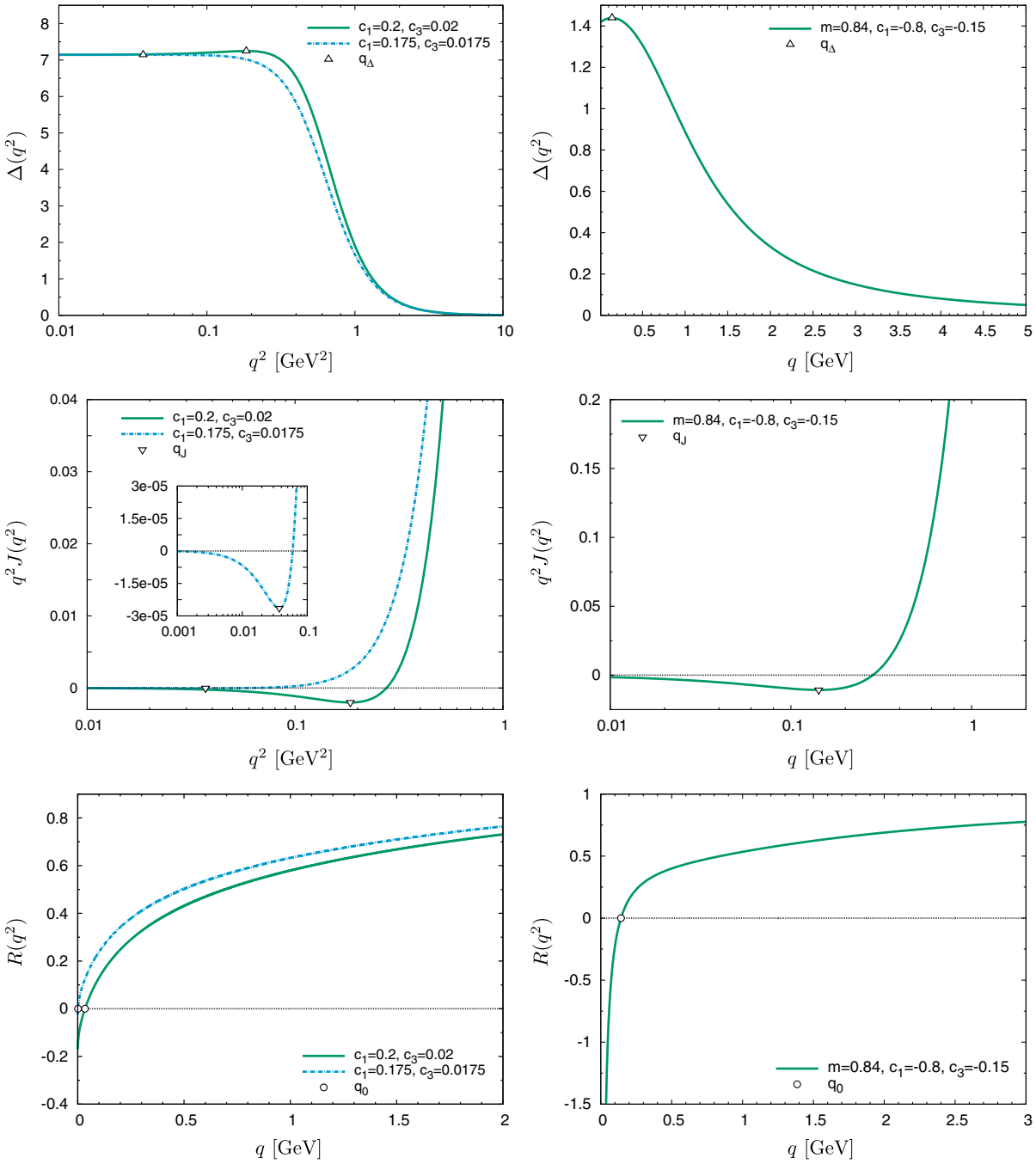

FIG. 2 (color online). The propagator $\Delta(q^2)$, its kinetic part $q^2J(q^2)$, and the quantity $R(q^2)$ calculated in $d = 3, 4$ for various values of the constants c_1 and c_3. In $d = 4$ we have $\mu = 4.3$ GeV, $m^2 = 0.14$ GeV^2, whereas in $d = 3$ we chose $m = 0.84$ GeV. Open up/down triangles and circles mark the position of the q_Δ, q_J, and q_0, respectively. Notice that, in this model, the locations of these three points coincide.

The kinetic part of the propagator, $q^2J(q^2) = \Delta^{-1}(q^2) - m^2$, is plotted in the middle panels of Fig. 2. Clearly, as mentioned earlier, due to the fact that m^2 is a constant, this quantity will display a (negative) minimum at exactly the same point where the peak of the propagator is located, $q_\Delta = q_J$. In the $d = 4$ case, the inset shows with more accuracy the extremely shallow minimum that is obtained for precisely those values of the c_i that cause the maximum of $\Delta(q^2)$ to flatten in the corresponding top panel.

Finally, in the bottom panels of Fig. 2, we plot $R(q^2)$. Again, the constancy of the gluon mass implies that this quantity will cross zero exactly at the location of the propagator's peak, displaying afterward the expected divergence as $q \to 0$. Notice that when $d = 4$ the zero

crossing is clearly detectable even in the region of parameters where the peak of the propagator (or the minimum of the kinetic part) is barely visible.

Summarizing, the fact that the ghost remains nonperturbatively massless has far-reaching consequences, which can be captured and studied at the qualitative level by the simple model (2.11). As we will see in what follows, the conclusions reached in this section are robust and will persist even in a fully nonperturbative setting.

III. FULL NONPERTURBATIVE ANALYSIS

In this section we proceed to corroborate by means of a genuine nonperturbative analysis the qualitative picture derived from the toy model of the previous section.

The material is organized in five interconnected subsections:

(i) First, some general issues are discussed, which facilitate the perusal of what follows.
(ii) Then, the detailed study of the ghost-loop contribution $J_c(q^2)$ follows, establishing its divergent behavior in the IR.
(iii) By employing the gluon mass equation and the lattice data for the gluon propagator, the full kinetic part, $q^2J(q^2)$ is determined, or, equivalently [by "subtracting" $q^2J_c(q^2)$] the gluonic contribution $q^2J_g(q^2)$.
(iv) The R projector of the three-gluon vertex is then studied in the relevant kinematic limit, revealing the announced divergence.
(v) Finally, a detailed numerical analysis is carried out.

A. Supplementary considerations

Before entering into the technical parts of this section, let us briefly go over certain conceptual subtleties related to the PT-BFM and its propagators [24,49].

Within the conventional formulation [69] of the SDE of the gluon propagator $\Delta(Q^2)$, while the *full* $J(q^2)$ comes out multiplied by the transverse projector $P_{\mu\nu}(q)$, thus reflecting the transversality of the full self-energy, no particular *subset* of the diagrams defining $J(q^2)$ displays this special property. Indeed, there is a nontrivial conspiracy of terms, stemming from each graph, which finally gives rise to a totally transverse self-energy. This fact is already captured at the level of the textbook one-loop calculation of the gluon self-energy [56]: it is only when the ghost-loop is added that one obtains the required transversality. Within this framework, therefore, the separation of "gluonic" and "ghost" contributions to $J(q^2)$ (say "J_g" and "J_c") using Feynman graphs as a criterion is ambiguous.

On the other hand, within the PT-BFM formalism, the SDE for the QB gluon propagator $\tilde{\Delta}$ possesses special transversality properties [see the discussion following Eq. (2.8) and the caption of Fig. 1]. As a result, one can meaningfully distinguish between two kinds of *individually transverse* contributions to $\tilde{J}(q^2)$—one stemming from the ghost graphs $(a_3)+(a_4)$, to be denoted by $\tilde{J}_c(q^2)$, and the rest stemming from gluonic graphs, to be denoted by $\tilde{J}_g(q^2)$. Thus,

$$q^2\tilde{J}_g(q^2)P_{\mu\nu}(q) = [(a_1)+(a_2)]_{\mu\nu} + [(a_5)+(a_6)]_{\mu\nu},$$
$$q^2\tilde{J}_c(q^2)P_{\mu\nu}(q) = [(a_3)+(a_4)]_{\mu\nu}. \tag{3.1}$$

Evidently,

$$\tilde{J}(q^2) = 1 + \tilde{J}_g(q^2) + \tilde{J}_c(q^2), \tag{3.2}$$

where the "1" on the rhs comes from the tree-level graph. As far as $\tilde{J}_g(q^2)$ is concerned, it is natural to expect that it will be IR finite, since it originates from the gluonic graphs shown in Fig. 1, namely, (single and double) integrals containing fully dressed (and IR-finite) gluon propagators.

At this point, one may use the fundamental relation of Eq. (2.8), which is valid for the full $J(q^2)$ and $\tilde{J}(q^2)$, in order to *define* the corresponding $J_g(q^2)$ and $J_c(q^2)$, namely,

$$J_{g,c}(q^2) = F(q^2)\tilde{J}_{g,c}(q^2). \tag{3.3}$$

As before,

$$J(q^2) = 1 + J_g(q^2) + J_c(q^2). \tag{3.4}$$

Finally, to establish a formal analogy with the toy model of the previous section, note that the correspondence with the terms appearing in Eq. (2.11) is $J_g \leftrightarrow c_1 J_{a_1}$ and $J_c \leftrightarrow c_3 J_{a_3}$.

We next comment briefly on the renormalization procedure that we follow when dealing with the ultraviolet divergences of the $d=4$ case. Specifically, we adopt the momentum subtraction (MOM) scheme, mainly because it is employed when renormalizing the lattice results that we use as inputs in our analysis.

Within the MOM scheme, the renormalized gluon propagator is required to assume its tree-level value at the subtraction point, i.e., must satisfy the condition $\Delta_{\rm R}^{-1}(\mu^2) = \mu^2$, for $\mu^2 \gg m^2$. The (quantum) kinetic terms $J_g^{\rm R}(q^2)$ and $J_c^{\rm R}(q^2)$ are then obtained from their unrenormalized counterparts through simple subtraction,

$$J_{g,c}^{\rm R}(q^2) = J_{g,c}(q^2) - J_{g,c}(\mu^2). \tag{3.5}$$

Evidently, $J_{g,c}^{\rm R}(\mu^2) = 0$. Thus, the full renormalized kinetic term is given by

$$J^{\rm R}(q^2) = 1 + J_g^{\rm R}(q^2) + J_c^{\rm R}(q^2), \tag{3.6}$$

with $J^{\rm R}(\mu^2) = 1$, consistent with the condition for $\Delta_{\rm R}^{-1}(\mu^2)$ mentioned above.

Finally, to keep this section as self-contained as possible, we list explicitly the three special values of the momentum q, first introduced in the context of the toy model:

(i) The location of the maximum of the gluon propagator, $\Delta(q^2)$, is denoted by q_Δ.
(ii) The location of the minimum of the kinetic term, $q^2J(q^2)$, is denoted by q_J.
(iii) The location of the zero crossing of the R projector is denoted by q_0.

B. Nonperturbative ghost loops and the minimum of the kinetic term

Our starting point are the two fully dressed diagrams (a_3) and (a_4) of Fig. 1, which, according to the above discussion, define $J_c(q^2)$ through

$$q^2J_c(q^2)P_{\mu\nu}(q) = F(q^2)[(a_3) + (a_4)]_{\mu\nu}. \tag{3.7}$$

Since the ghost remains massless nonperturbatively, the resulting contribution will be IR divergent, as happens in the one-loop perturbative case.

To see this in detail, let us focus on the rhs of Eq. (3.7). Factoring out the trivial color structure δ^{ab}, one has

$$\begin{aligned}(a_3)_{\mu\nu} &= -g^2C_A\int_k (k+q)_\mu D(k)D(k+q)\tilde{\Gamma}_\nu(k+q,-q,-k),\\ (a_4)_{\mu\nu} &= g^2C_Ag_{\mu\nu}\int_k D(k).\end{aligned} \tag{3.8}$$

In the above equations, $\tilde{\Gamma}_\mu(r,q,p)$ is the PT-BFM vertex describing the interaction of a background gluon with a ghost and an antighost; unlike the conventional ghost-gluon vertex, its tree-level expression is symmetric in the ghost momenta, $\tilde{\Gamma}^{(0)}_\mu(r,q,p) = (r-p)_\mu$. In addition, we have introduced the d-dimensional measure $\int_k \equiv \mu^\epsilon/(2\pi)^d\int \mathrm{d}^dk$, where μ is the 't Hooft mass and $\epsilon = 4-d$.

Since, due to the PT-BFM properties, $\tilde{\Gamma}_\mu$ satisfies the WI [24,49]

$$q^\mu\tilde{\Gamma}_\mu(r,q,p) = D^{-1}(p) - D^{-1}(r), \tag{3.9}$$

one may establish immediately the transversality of this subset of diagrams, as anticipated by the presence of the projector $P_{\mu\nu}(q)$ on the lhs of Eq. (3.7).

One may now introduce an ansatz for $\tilde{\Gamma}_\mu$, that satisfies automatically the above WI, namely,

$$\tilde{\Gamma}_\mu(r,q,p) = \frac{(r-p)_\mu}{r^2-p^2}[D^{-1}(r^2) - D^{-1}(p^2)]. \tag{3.10}$$

A corresponding construction for the conventional ghost-gluon vertex would be less forthcoming, given the type of STI that the latter satisfies [56].

This procedure fixes completely the longitudinal part of the vertex but leaves its transverse component, $\tilde{\Gamma}^t_\mu = \mathcal{A}(r,p)[(r\cdot q)p_\mu - (p\cdot q)r_\mu]$, undetermined. However, under rather mild assumptions on the behavior of $\mathcal{A}(r,p)$, this latter term is subleading in the IR (see Appendix B), and its effects may be neglected at this stage.[7]

Before proceeding with the actual calculation, let us clarify a potentially confusing point. The terminology we use to characterize the two distinct Lorentz structures of the ghost vertex goes back to the pioneering work of Ball and Chiu [72]: the automatically conserved part of the vertex (i.e., the one annihilated when contracted by q^μ) is referred to as the transverse part, in exact analogy to what happens with the photon (or gluon) propagator. By the same logic, the part that contributes to the WI is denominated longitudinal. Clearly, in the case of the photon propagator, given that there is only one momentum available (q), the longitudinal part $q_\mu q_\nu$ vanishes when contracted with the transverse $P_{\mu\nu}(q)$. However, in the case of the vertex, this last property is no longer true: the contraction of its longitudinal part by $P_{\mu\nu}(q)$ does not vanish. We will therefore use this terminology under the proviso just mentioned. The above comment applies also to the case of the three-gluon vertex or any other vertex with a nontrivial Lorentz structure (see, e.g., Ref. [73]).

Substituting the vertex (3.10) into the first equation of Eq. (3.8), and taking the trace of both sides, one obtains

$$q^2J_c(q^2) = C_dF(q^2)[4T(q^2) + q^2S(q^2)], \tag{3.11}$$

where we have defined

$$C_d = \frac{g^2C_A}{2(d-1)}, \tag{3.12}$$

and

$$\begin{aligned}T(q^2) &= \int_k \frac{F(k+q)-F(k)}{(k+q)^2-k^2} + \left(\frac{d}{2}-1\right)\int_k\frac{F(k)}{k^2},\\ S(q^2) &= \int_k\frac{F(k)}{k^2(k+q)^2} - \int_k\frac{F(k+q)-F(k)}{k^2[(k+q)^2-k^2]}.\end{aligned} \tag{3.13}$$

Let us now study at the IR behavior of these quantities. For the term S, one finds

$$\begin{aligned}S(q^2) &\underset{q^2\to 0}{\longrightarrow} \int_k\frac{F(k)}{k^4} - \int_k\frac{1}{k^2}\frac{\partial F(k)}{\partial k^2} + \mathcal{O}(q^2)\\ &\sim \int_k\frac{F(k)}{k^4} - \int_0^\infty \mathrm{d}y y^{d/2-2}F'(y) + \mathcal{O}(q^2),\end{aligned} \tag{3.14}$$

[7]Of course, in $d=4$ the omission of the transverse term affects the ultraviolet properties of the resulting SDE, forcing subtractive instead of multiplicative renormalization [70,71].

where in the last step we have passed to spherical coordinates, with $y = k^2$ [see Eq. (B4)].

The first integral on the rhs contains the divergence discussed in the previous section. This can be seen by simply setting $F(y) = 1$, in which case one finds a logarithmic ($d = 4$) or a linear ($d = 3$) divergence. Given that the full $F(y)$ saturates at a constant value in the IR, its presence does not qualitatively modify the behavior of the integral with respect to the case when $F(y) = 1$; roughly speaking, it simply changes its prefactor from 1 to $F(0)$.

It is now relatively straightforward to establish that the second integral in Eq. (3.14) is subleading compared to the first one, as a result of the fact that $F(y)$ is a finite function in the entire range of momenta. Indeed, in $d = 4$, integration by parts shows that it is simply equal to $F(0)$, and, therefore, it contributes a finite constant.

In $d = 3$, let us assume that $F' \sim y^{-a}$; then one may naturally distinguish three cases, depending on the value of the exponent a:

(i) If $a < 1/2$, it is clear that the integral is finite, and evidently subleading.
(ii) If $1/2 \leq a < 1$, the integral diverges, but with a degree of divergence inferior to $1/q$ (or $y^{-1/2}$).
(iii) If $a \geq 1$, the second integral diverges faster than the first.

Now, given that from $F' \sim y^{-a}$ one deduces that $F(y) \sim (1-a)^{-1} y^{1-a} + C$, if $a \neq 1$, and $F(y) \sim C + \ln y$, if $a = 1$, the finiteness of $F(y)$ imposes the restriction $a < 1$. Therefore, one is driven to the case (i) or (ii), and, consequently, the second integral may be finite or divergent in the IR but is certainly subleading compared to the first.

Next, consider the term $T(q^2)$; following a similar procedure, we obtain

$$T(q^2) \underset{q^2\to 0}{\to} T(0) = \int_k \frac{\partial F(k^2)}{\partial k^2} + \left(\frac{d}{2} - 1\right) \int_k \frac{F(k)}{k^2}. \quad (3.15)$$

It is now immediate to recognize that $T(0)$ vanishes, since Eq. (3.15) is a particular case of the so-called "seagull identity" [74],

$$\int_k k^2 \frac{\partial f(k^2)}{\partial k^2} + \frac{d}{2} \int_k f(k^2) = 0, \quad (3.16)$$

valid in dimensional regularization.[8]

Then, employing that $T(0) = 0$, and after repeated use of Eq. (3.16), one finds that

$$T(q^2) \underset{q^2\to 0}{\to} -\frac{1}{12}(d-2) q^2 \int_k \frac{1}{k^2} \frac{\partial F(k)}{\partial k^2} + \mathcal{O}(q^4); \quad (3.17)$$

that is, we end up with the first integral on the rhs of Eq. (3.14), which is subleading.

Thus, if we split J_c in a part that contains the leading contribution in the IR, $J_c^{\ell}(q^2)$, and the rest that is subleading, $J_c^{s\ell}(q^2)$,

$$J_c(q^2) = J_c^{\ell}(q^2) + J_c^{s\ell}(q^2), \quad (3.18)$$

we conclude that the leading divergent contribution is that contained in the first term of $S(q^2)$, namely,

$$J_c^{\ell}(q^2) = C_d F(q^2) \int_k \frac{F(k)}{k^2 (k+q)^2}. \quad (3.19)$$

On the other hand, $J_c^{s\ell}(q^2)$ consists of all those terms that have been discarded throughout the procedure described above. It may be computed numerically, but its detailed form is of no immediate interest, and it will be simply included in the full curve describing $J_c(q^2)$.

The divergent nature of $J_c(q^2)$ causes the kinetic term $q^2 J(q^2)$ to acquire a minimum in the IR region, as can be demonstrated by following basically the arguments related with Eq. (2.15). In particular, using Eqs. (3.4) and (3.18), one has

$$[q^2 J(q^2)]' = J_c^{\ell}(q^2) + \{1 + q^2 J'(q^2) + J_c^{s\ell}(q^2)\}. \quad (3.20)$$

Now, as happens in the case of the toy model, (i) the quantity in curly brackets is subleading in the IR, and (ii) the above derivative is positive in the ultraviolet, since $q^2 J(q^2)$ increases [and so, $\Delta(q^2)$ decreases]. Thus, the derivative reverses its sign, becoming zero at the point q_J, namely,

$$[q^2 J(q^2)]'_{q=q_J} = 0. \quad (3.21)$$

We must emphasize at this point that even though the existence of the minimum is established by means of the above argument, its location cannot be accurately determined because we do not know all terms appearing in the curly bracket of Eq. (3.20). Therefore, q_J *cannot* be computed *directly*; however, in the next subsection, we will determine its value *indirectly*, from the (better known) combination $\Delta^{-1}(q^2) - m^2(q^2)$.

C. Maximum of $\Delta(q^2)$ and indirect determination of $J_g(q^2)$

Let us now examine whether the maximum of the gluon propagator established in Sec. II in the context of the toy model persists in the full nonperturbative treatment.

Evidently, the main qualitative difference between the two situations is that now the gluon mass is not a constant but a function of the momentum, $m^2(q^2)$. Specifically, the corresponding $[\Delta^{-1}(q^2)]'$ reads

[8]The origin of Eq. (3.16) is simple integration by parts, where the surface term is dropped by appealing to the analyticity properties of dimensional regularization. Its main function in the context of gluon mass generation is to enforce the complete cancellation of all quadratic (seagull-type) divergences.

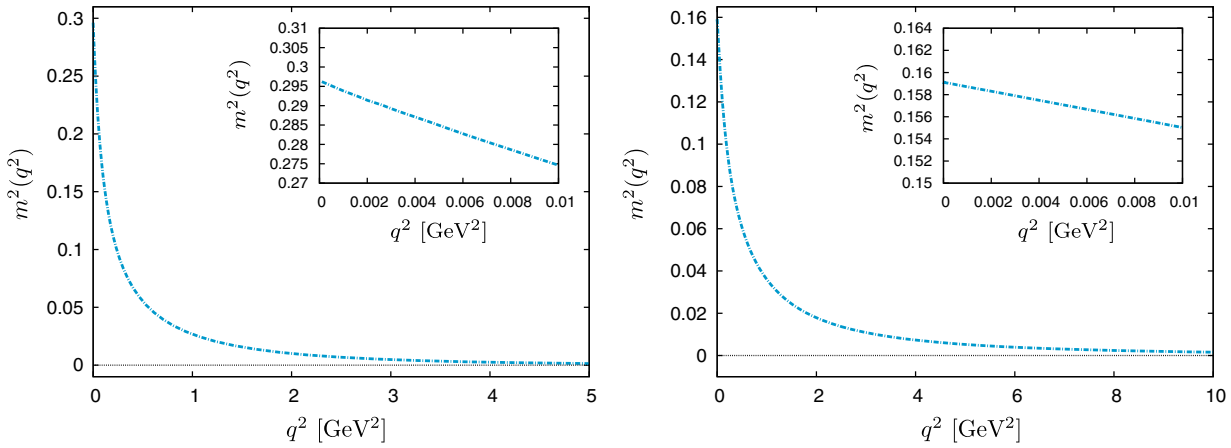

FIG. 3 (color online). Solutions of the mass equation for the SU(2) (left) and SU(3) (right) gauge groups. In the insets we show the deep IR region of the same curves.

$$[\Delta^{-1}(q^2)]' = [q^2 J(q^2)]' + [m^2(q^2)]'. \tag{3.22}$$

Now, if the quantity $[m^2(q^2)]'$ is a "well-behaved" function, then the arguments following Eq. (3.20) would again go through here. In particular, the existence of a zero is guaranteed, provided that the IR divergence of $J_c^\ell(q^2)$ is not cancelled exactly by a similar divergence (with opposite sign) contained in $[m^2(q^2)]'$.

To discard this remote possibility, we turn to the dynamical equation that governs $m^2(q^2)$, which, in its exact form, reads [37]

$$m^2(q^2) = -g^2 C_A D(q^2) \int_k m^2(k^2) \Delta^\mu_\rho(k) \Delta^{\nu\rho}(k+q) \mathcal{K}_{\mu\nu}(k,q), \tag{3.23}$$

with the kernel given by

$$\mathcal{K}_{\mu\nu}(k,q) = [(k+q)^2 - k^2]\{1 - [Y(k+q) + Y(k)]\} g_{\mu\nu} + [Y(k+q) - Y(k)](q^2 g_{\mu\nu} - 2 q_\mu q_\nu) \tag{3.24}$$

and Y defined through

$$Y(k^2) = \frac{g^2 C_A}{4k^2} k_\alpha \int_r \Delta^{\alpha\rho}(r) \Delta^{\beta\sigma}(r+k) \Gamma_{\sigma\rho\beta}(-r-k, r, k), \tag{3.25}$$

where $\Gamma_{\sigma\rho\beta}$ is the full three-gluon vertex.

This equation has been studied in $d = 4$, under certain simplifying assumptions regarding the structure of the function $Y(k^2)$. In particular, Y was replaced by its lowest perturbative approximation, given by

$$Y_{\rm R}(k^2) = -\frac{\alpha_s C_A}{4\pi} \frac{15}{16} \log \frac{k^2}{\mu^2}, \tag{3.26}$$

with α_s the value of the strong coupling at the subtraction point chosen. In practice, this simple approximation is improved by letting $Y \to CY$, where C is an arbitrary constant, modeling further corrections that may be added to the "skeleton" result of Eq. (3.26).

From Eq. (3.23) one obtains positive-definite solutions for the gluon mass function, at least within a reasonable range of physical momenta. In particular, we fix $\mu = 4.3$ GeV and use for $\alpha_s(\mu)$ the MOM value obtained from the corresponding formulas of Ref. [75], namely, $\alpha_s(\mu) = 0.22$. Then, for $C = 9.2$, the function $m^2(q^2)$ is positive and monotonically decreasing in the range of momenta between[9] 0 and 5.5 GeV.

Evidently, this behavior (see Fig. 3) excludes the possibility of $m^2(q^2)$ having a divergent (and positive) derivative at the origin. Therefore, we conclude that the rhs of Eq. (3.22) must reverse its sign at some point (q_Δ), where the corresponding gluon propagator will display a maximum. Of course, the presence of the term $[m^2(q^2)]'$ in Eq. (3.22) prevents the coincidence between q_Δ and q_J, unless $[m^2(q^2)]'_{q=q_J} = 0$; but this possibility is discarded, due to the monotonic nature of $m^2(q^2)$. Thus, we conclude that $q_\Delta \neq q_J$.

One may go one step further and demonstrate that, in fact, $q_J < q_\Delta$. Indeed, evaluating both sides of Eq. (3.22) at the point q_J, where the first term on the rhs vanishes, one has

$$[\Delta^{-1}(q_J^2)]' = [m^2(q_J^2)]' < 0, \tag{3.27}$$

since $m^2(q^2)$ is monotonically decreasing. Thus, at q_J the derivative of $\Delta^{-1}(q^2)$ is still negative and has yet to reach its point of zero crossing, a fact that places q_Δ to the right of q_J on the axis of momenta. As will be shown in Fig. 7, this particular inequality is in complete agreement with the numerical analysis presented in the last subsection.

[9]Past this point $m^2(q^2)$ turns negative (but its magnitude is extremely small), reaching finally zero from negative values [76]. The necessary refinements for rectifying this will be reported elsewhere.

In addition to consolidating the above considerations, the (approximate) knowledge of $m^2(q^2)$, when combined with the lattice information on the full $\Delta(q^2)$ [1–5], may furnish the full $q^2J(q^2)$, simply from

$$q^2J(q^2) = \underbrace{\Delta^{-1}(q^2)}_{\text{lattice}} - \underbrace{m^2(q^2)}_{\text{Eq. (3.23)}}. \tag{3.28}$$

When coupled with the result (3.11), the procedure outlined above allows for a gauge-invariant identification of the two components contributing to the gluon propagator. Specifically, the gluon kinetic term can be obtained from [see also Eq. (3.4)]

$$q^2 + q^2J_g(q^2) = \underbrace{\Delta^{-1}(q^2)}_{\text{lattice}} - \underbrace{m^2(q^2)}_{\text{Eq. (3.23)}} - \underbrace{q^2J_c(q^2)}_{\text{Eq. (3.11)}}. \tag{3.29}$$

The results of these operations will be discussed in the last subsection.

D. *R* projector

The final step is to link the gluon kinetic term with lattice simulations of the three-gluon vertex. To this end, let us recall that the typical quantity employed on the lattice projects the full vertex on its tree-level value, dividing out, at the same time, external leg corrections [8,9]. Specifically, for the three-gluon vertex in the Landau gauge, one considers

$$R(q,r,p) = \frac{\mathcal{N}(q,r,p)}{\mathcal{D}(q,r,p)}, \tag{3.30}$$

where

$$\begin{aligned}\mathcal{N}(q,r,p) &= \Gamma^{(0)}_{\alpha\mu\nu}(q,r,p)P^{\alpha\rho}(q)P^{\mu\sigma}(r)P^{\nu\tau}(p)\\ &\quad\times\Gamma_{\rho\sigma\tau}(q,r,p),\\ \mathcal{D}(q,r,p) &= \Gamma^{(0)}_{\alpha\mu\nu}(q,r,p)P^{\alpha\rho}(q)P^{\mu\sigma}(r)P^{\nu\tau}(p)\\ &\quad\times\Gamma^{(0)}_{\rho\sigma\tau}(q,r,p).\end{aligned} \tag{3.31}$$

As already mentioned, the ratio (3.30) can be characterized by the modulo of two independent momenta and the angle formed between them, so that one has $R = R(q^2, r^2, \varphi)$. Then, the quantity of interest corresponds to the so-called "orthogonal configuration," $\varphi = \pi/2$, where, in addition, we take the limit $r^2 \to 0$, namely, $R(q^2, 0, \pi/2)$.

In this particular limit, R may be obtained from the combination [77]

$$R(q^2,0,\pi/2) = X_7(q^2,0,\pi/2) + q^2X_9(q^2,0,\pi/2). \tag{3.32}$$

In the formula above, $X_{7,9}$ represent two of the 10 longitudinal form factors which characterize the longitudinal part of the vertex (see Appendix A); their explicit forms can be determined by solving the STI satisfied by the vertex and reads [72]

$$\begin{aligned}X_7(q,r,p) = \frac{1}{4}\{&2[F(q^2)J(p^2)a_{rqp} + F(p^2)J(q^2)a_{rpq}] + r^2[F(p^2)J(r^2)b_{qpr} + F(q^2)J(r^2)b_{pqr}]\\ &+ (q^2-p^2)[F(r^2)J(q^2)b_{prq} + F(q^2)J(p^2)b_{rqp} - F(r^2)J(p^2)b_{qrp} - F(p^2)J(q^2)b_{rpq}]\\ &+ 2(q\cdot r)F(p^2)J(q^2)d_{rpq} + 2(r\cdot p)F(q^2)J(p^2)d_{rqp}\},\end{aligned} \tag{3.33}$$

$$\begin{aligned}X_9(q,r,p) = \frac{F(r^2)}{q^2-p^2}&[J(q^2)a_{prq} - J(p^2)a_{qrp}\\ &+ (r\cdot p)J(p^2)d_{qrp} - (q\cdot r)J(q^2)d_{prq}],\end{aligned} \tag{3.34}$$

with a, b, and d representing the form factors appearing in the tensorial decomposition of the gluon-ghost kernel H [72],

$$\begin{aligned}H_{\nu\mu}(p,r,q) = {}& g_{\mu\nu}a_{qrp} - r_\mu q_\nu b_{qrp} + q_\mu p_\nu c_{qrp} + q_\nu p_\mu d_{qrp}\\ &+ p_\mu p_\nu e_{qrp},\end{aligned} \tag{3.35}$$

and a_{qrp} a short-hand notation for $a(q,r,p)$, etc. Note finally that, in this particular kinematic limit, the four (undetermined) transverse components of the three-gluon vertex (see Appendix A) drop out completely.

Let us now study the IR behavior of $R(q^2,0,\pi/2)$. Consider first the X_7 term; in the orthogonal configuration, one has

$$p^2 = q^2 + r^2; \quad (q\cdot r) = 0; \quad (q\cdot p) = -q^2; \quad (r\cdot p) = -r^2; \tag{3.36}$$

then, taking the limit $r^2 \to 0$, Eq. (3.33) gives the result

$$X_7(q^2,0,\pi/2) = F(q^2)J(q^2)a(0,q,-q). \tag{3.37}$$

For X_9, which in the orthogonal configuration reads

$$\begin{aligned}X_9(q^2,r^2,\pi/2) = {}& F(r^2)J(p^2)d_{qrp}\\ &- \frac{F(r^2)}{r^2}[J(q^2)a_{prq} - J(p^2)a_{qrp}],\end{aligned} \tag{3.38}$$

the corresponding treatment is slightly more involved. The first term appearing in Eq. (3.38) can be simplified using the identity[10] [78]

$$F(r^2)[a_{qrp} - (q\cdot r)b_{qrp} + (q\cdot p)d_{qrp}] = F(q^2)[a_{rqp} - (q\cdot r)b_{rqp} + (p\cdot r)d_{rqp}], \quad (3.39)$$

yielding in the limit of interest

$$q^2F(0)d(q,0,-q) = F(0) - F(q^2)a(0,q,-q). \quad (3.40)$$

In arriving at the above result, we used the fact that, in the Landau gauge, $a(q,0,-q)$ maintains to all orders its tree-level value [79], i.e., $a(q,0,-q)=1$.

For the second term in Eq. (3.38), one needs to perform a Taylor expansion around $r^2=0$ of both a_{prq} and $J(p)a_{qrp}$; using

$$a_{prq} \underset{r^2\to 0}{=} 1 + r^2\frac{\partial}{\partial r^2}a_{prq}\Big|_{r^2=0} + \mathcal{O}(r^4),$$
$$J(p)a_{qrp} \underset{r^2\to 0}{=} J(q) + r^2\frac{\partial}{\partial r^2}[a_{qrp}J(p)]\Big|_{r^2=0} + \mathcal{O}(r^4), \quad (3.41)$$

we obtain

$$-\frac{F(r^2)}{r^2}[J(q^2)a_{prq} - J(p^2)a_{qrp}] \underset{r^2\to 0}{=} F(0)\left[J'(q^2) + J(q^2)\frac{\partial}{\partial r^2}(a_{qrp} - a_{prq})\big|_{r^2=0}\right], \quad (3.42)$$

where the prime denotes, as usual, derivatives with respect to q^2. Thus, inserting Eqs. (3.40) and (3.42) in Eq. (3.38), one derives the expression

$$q^2X_9(q^2,0,\pi/2) = J(q^2)[F(0) - F(q^2)a(0,q,-q)] + F(0)q^2J'(q^2) + \mathcal{O}(q), \quad (3.43)$$

with $\mathcal{O}(q)$ indicating subleading terms, specifically the derivative of $a_{qrp} - a_{prq}$ appearing in Eq. (3.42).

Substituting the results (3.37) and (3.43) in Eq. (3.32), we obtain the final expression (we only indicate q^2 in the argument)

$$R(q^2) = F(0)[q^2J(q^2)]' + R^{s\ell}(q^2), \quad (3.44)$$

which shows that the behavior of R in the deep IR is determined solely by J,

$$R(q^2) \underset{q^2\to 0}{\sim} F(0)J(q^2). \quad (3.45)$$

The term $R^{s\ell}(q^2)$ denotes the subleading corrections not contained in the first term. Therefore, from Eq. (3.19), the dominant contribution in that limit is

$$R(q^2) \underset{q^2\to 0}{\sim} C_dF^2(0)\int_k \frac{F(k)}{k^2(k+q)^2}. \quad (3.46)$$

If we now assume that the ultraviolet behavior of $R(q^2)$ is qualitatively described by Eq. (2.23), then the $R(q^2)$ of Eq. (3.44) must vanish at a point q_0, $R(q_0^2)=0$, and then eventually diverge in the IR, according to Eq. (3.46).

The location of q_0 with respect to the other two special points, q_Δ and q_J, is not possible to determine. Since, from Eq. (3.22) we have $[q_\Delta^2J(q_\Delta^2)]' = -[m^2(q_\Delta^2)]'$, the value of $R(q^2)$ at these two points is given by

$$R(q_\Delta^2) = R^{s\ell}(q_\Delta^2) - F(0)[m^2(q_\Delta^2)]',$$
$$R(q_J^2) = R^{s\ell}(q_J^2). \quad (3.47)$$

For the point q_0 to coincide with either q_Δ or q_J, the corresponding rhs in Eq. (3.47) ought to vanish; this possibility, however, cannot be checked analytically, due to the lack of knowledge of the function $R^{s\ell}$. Of course, in the toy model, $R^{s\ell}$ is identically zero, and so is the derivative of the mass, forcing the equality between these three special points. The available lattice data for SU(2) in $d=3$ [2,8,9] seem to suggest a relative proximity between q_0 and q_Δ, with $q_\Delta \approx q_0 \approx 380$ MeV; of course, the lattice parameters used for computing the two- and three-point functions are rather different, so this comparison is only suggestive at this point.

E. Numerical results

We finally carry out a detailed numerical study of all the quantities introduced in the previous four subsections.

Let us start by evaluating from the the full nonperturbative ghost-loop contribution (3.7) to the gluon kinetic term $q^2J(q^2)$ in the four-dimensional case. For evaluating all the terms appearing in Eqs. (3.11) and (3.13), we used as input a functional fit to the SU(2) [2] and SU(3) [3] unquenched lattice data for the ghost dressing function. Specifically, we set (see also Fig. 4),

$$F^{-1}(q^2) = 1 + \frac{9}{4}\frac{C_Ag_1^2}{48\pi^2}\ln\frac{1}{\mu^2}\left(q^2 + \frac{\rho_1 m_0^4}{q^2+\rho_2 m_0^2}\right), \quad (3.48)$$

with $m_0 = 520$ MeV, $g_1^2 = 8.65$, $\rho_1 = 0.25$, and $\rho_2 = 0.64$ for SU(3) and $m_0 = 815$ MeV, $g_1^2 = 14.81$, $\rho_1 = 0.023$, and $\rho_2 = 0.20$ for SU(2). In both cases we have $\mu = 4.3$ GeV.

[10] This identity is a direct consequence of the STI satisfied by the ghost kernel H and constitutes a necessary condition for obtaining a consistent solution of the STIs of the three-gluon vertex [78].

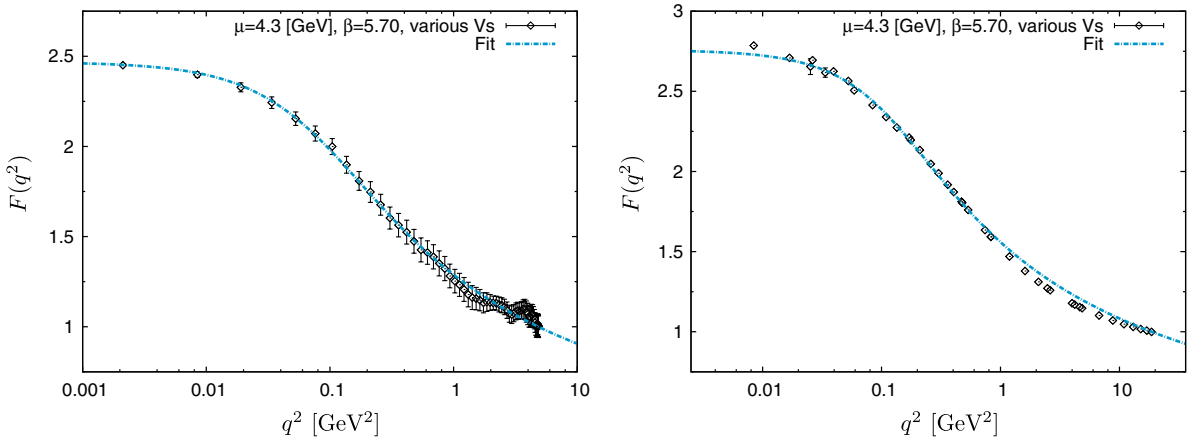

FIG. 4 (color online). The functional fit given in Eq. (3.48) to the ghost dressing functions for SU(2) (left) and SU(3) (right). Lattice data are taken from Refs. [1,2], and [3], respectively.

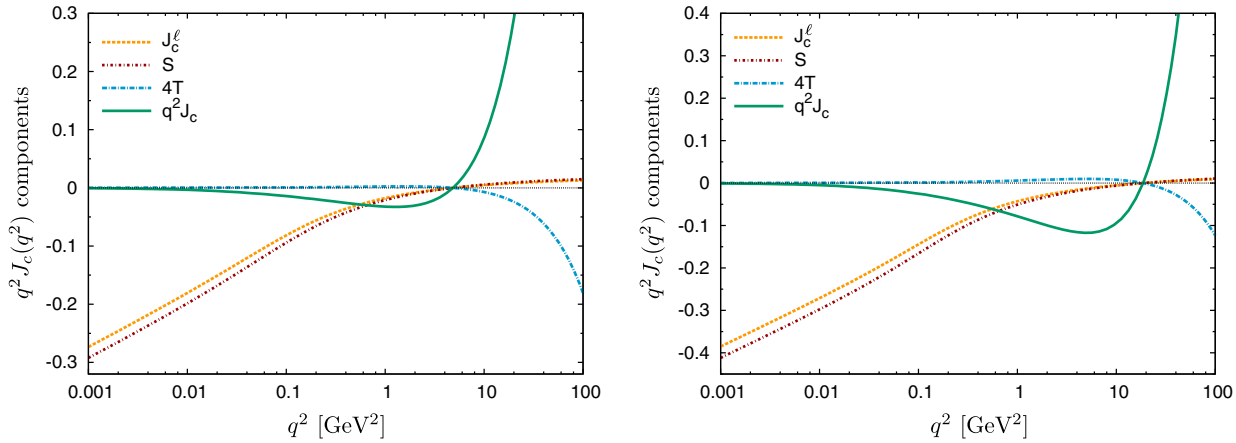

FIG. 5 (color online). The ghost-loop contribution, $q^2 J_c(q^2)$, to the gluon kinetic term $q^2 J(q^2)$ for the SU(2) (left) and SU(3) (right) gauge groups.

The results are shown in Fig. 5, where, as anticipated, the IR logarithmic divergence, clearly identified by the linear behavior (in log scale) of the S term, persists in both cases even in a fully nonperturbative setting.

Now, according to the reasoning developed so far, and as a consequence of this particular divergence, the lattice data for the gluon propagator ought to display a maximum, located in the (deep) IR region. Such a maximum appears to be indeed encoded in the lattice data for the gluon propagator, which seem to show a suppression of the deep IR points. This particular feature is displayed in the insets appearing in the panels of Fig. 6, where, together with the lattice data, we also plot different fitting curves, in which the position of the maximum is varied. To be sure, the maximum is not easy to discern and is located in a region of momenta where the lattice simulations are plagued with considerable errors, due to a variety of technical difficulties. We emphasize that the set of gluon propagators presented here are not the output of a full SDE analysis[11] but rather a particular fit of the existing lattice data, which is designed to exhibit the theoretical feature that we advocate, namely, the (rather flat) maximum. These propagators will be used as an input below, in order to deduce or confirm additional aspects of the theoretical picture put forth in the previous analysis.

We next turn to the indirect determination of $q^2 J(q^2)$ from Eq. (3.28), using as basic input the family of curves for $\Delta(q^2)$ obtained in the previous step. To that end, we first

[11]The reason why a full SDE analysis is beyond our powers has already been mentioned earlier; it essentially boils down to the fact that we do not have satisfactory control over some of the basic ingredients appearing in the integral equation governing $J(q^2)$. In particular, and contrary to what happens in the case of the mass equation, the equation for $J(q^2)$ (not reported here) involves the fully dressed four-gluon vertex, for which the structure is very poorly known. This is why one has to settle for an "indirect" determination of $J(q^2)$, as opposed to a direct one, which would amount to solving the full system for $m^2(q^2)$ and $J(q^2)$ simultaneously.

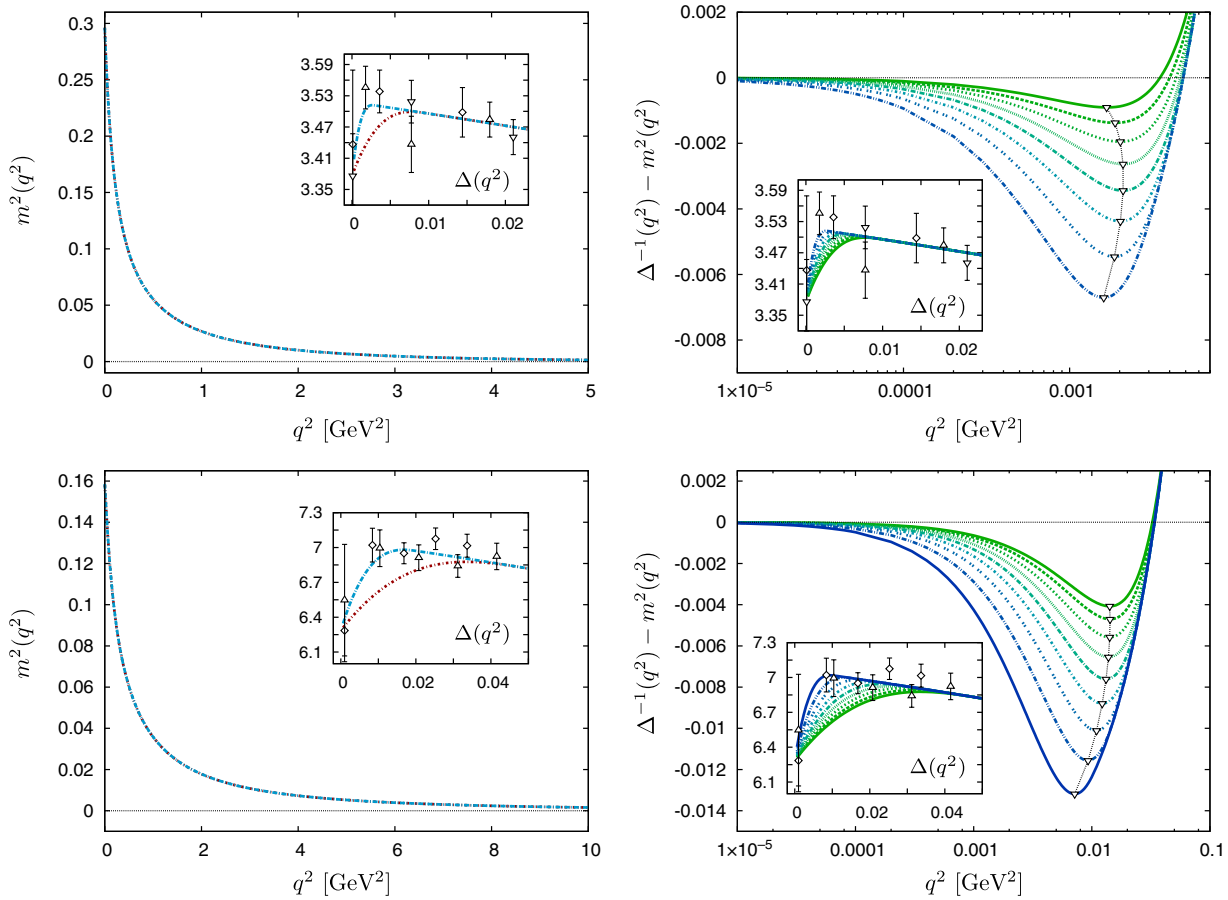

FIG. 6 (color online). The dynamical gluon mass (left panels) and the propagator's full kinetic part $\Delta^{-1}(q^2) - m^2(q^2)$ (right panels) for the SU(2) (top) and SU(3) (bottom) gauge groups. Whereas the solutions of the mass equation are clearly insensitive to the presence of a maximum in the propagator, as shown for two representative cases, the full kinetic term develops a negative minimum (q_J), for which the position is marked in the right panels by open (down) triangles. Insets show in all cases the IR behavior of the various propagator fits used as input, together with the corresponding lattice data of Refs. [1,2], and [3].

establish that, when the latter curves are used as input for the mass equation (3.23), the resulting masses turn out to be completely independent of the location and the size of the maximum of the propagator (left panels of Fig. 6). Thus, while $\Delta(q^2)$ is varied on the rhs of Eq. (3.28), the corresponding $m^2(q^2)$ remains the same for all cases. The result of this procedure is shown on the right panels of Fig. 6; each $q^2J(q^2)$ so obtained vanishes at the origin, decreases in the deep IR, and reaches a negative minimum before crossing zero and turning positive. The location of the corresponding minimum, q_J, is clearly marked for each separate case.

Evidently, since every $\Delta(q^2)$ has a maximum at a point q_Δ, and since from each such $\Delta(q^2)$ we obtain a $q^2J(q^2)$ with a minimum at a point q_J, one may plot q_J as a function of q_Δ. The resulting relation is shown in Fig. 7. The shaded area serves as a reference, corresponding to the case $q_J \geq q_\Delta$. The plot clearly indicates that all points lie below this region, demonstrating that, indeed, $q_J < q_\Delta$, as previously anticipated using Eq. (3.27).

Notice that, as an important byproduct of this analysis, we are able to disentangle gauge invariantly the ghost and gluon contributions to the kinetic term and the propagator. This is shown in Fig. 8, where one can appreciate that the gluon contribution is dominant; however, in the crucial region below 1 GeV^2, there are still sizeable contributions from ghost terms. It should be also noticed that there is a substantial difference between the SU(3) and SU(2) gauge groups, in the sense that the relative size disparity between the various components is more moderate in the SU(2) case. Finally, in Fig. 9 we show the tree-level and quantum part of the gluon kinetic term; notice that in this case, any structure appearing in the quantum term gets completely washed out by the tree-level term (obviously absent for the ghost contributions).

As Eq. (3.44) reveals, the position of the minimum of the full kinetic term provides an estimate for the momentum q_0 where the three-gluon projector $R(q^2, 0, \pi/2)$ crosses zero and reverses sign. In the SU(2) case, this turns out to be located quite deep in the IR, as one gets (see Fig. 10) $q_0 \approx 44$ MeV, while for SU(3) we obtain $q_0 \approx 132$ MeV.

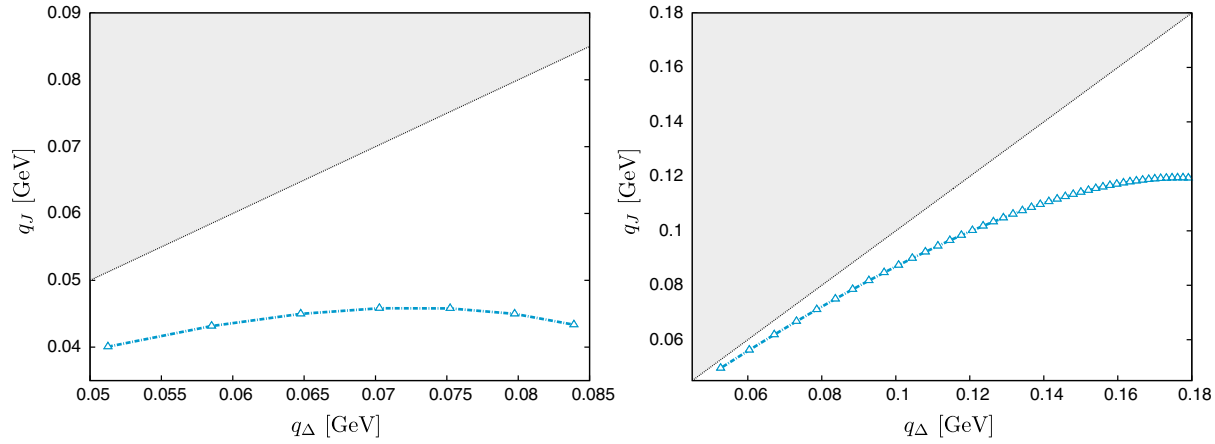

FIG. 7 (color online). The points q_J plotted as a function of the points q_Δ for the SU(2) (left) and SU(3) (right) gauge groups. The shaded area on both panels corresponds to the region $q_J \geq q_\Delta$.

At this point, we can use the relation (see, e.g., Ref. [80])

$$q = \frac{2}{a}\sin\frac{\pi k}{L} \times 197.3 \text{ MeV fm}, \tag{3.49}$$

with a the lattice size (in fermi), L the number of lattice sites, and $k \leq L$ an integer locating the different sites in the corresponding lattice direction, in order to convert the numbers obtained above into the lattice volumes needed to

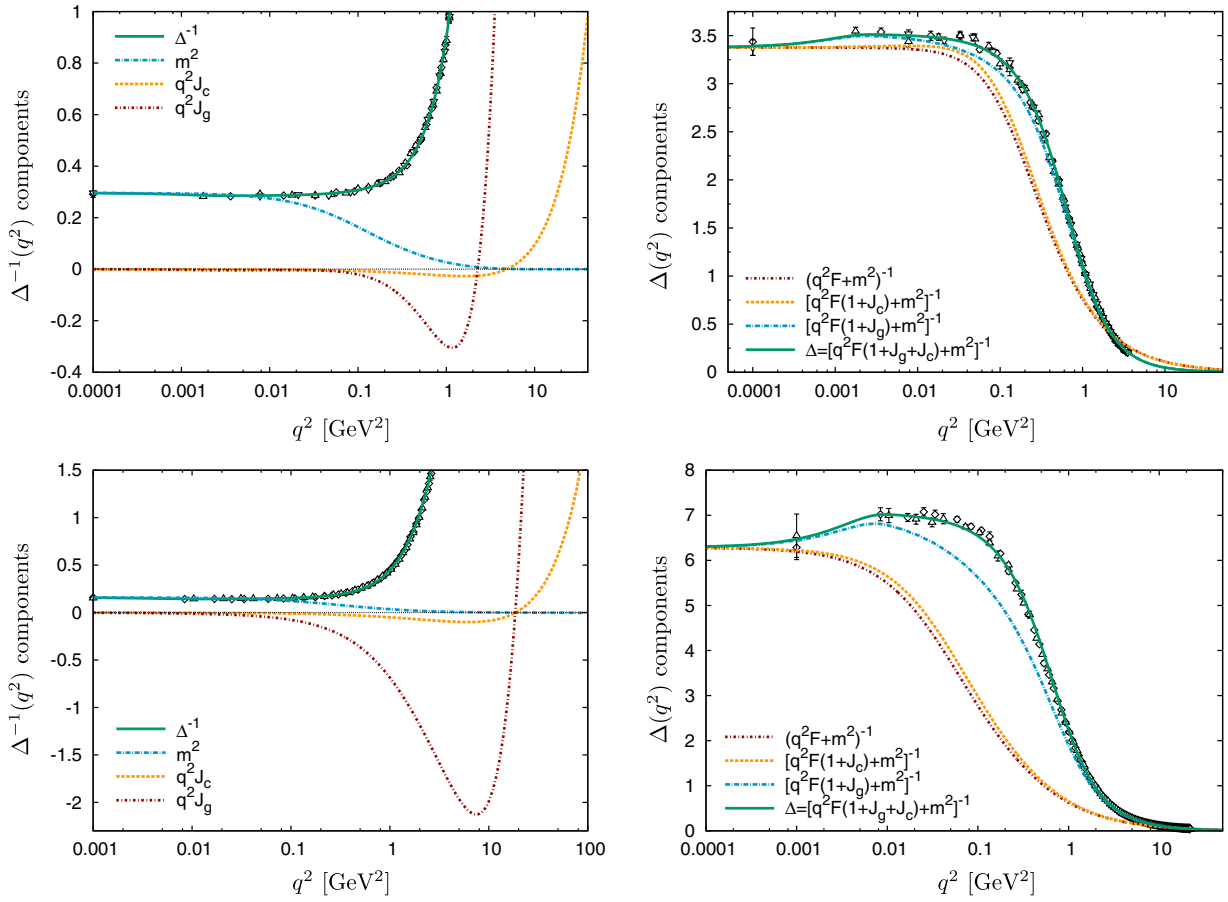

FIG. 8 (color online). The gauge-invariant decomposition of the ghost and gluon components of the gluon propagator (right panels) and its inverse (left panels) for the SU(2) (top) and SU(3) (bottom) gauge groups. The quenched lattice data for the SU(2) and SU(3) gluon propagators are taken from Refs [1,2], and [3], respectively. Notice that in the left panels the tree-level contribution to the gluon kinetic term has been suppressed; its effect can be seen clearly in Fig. 9.

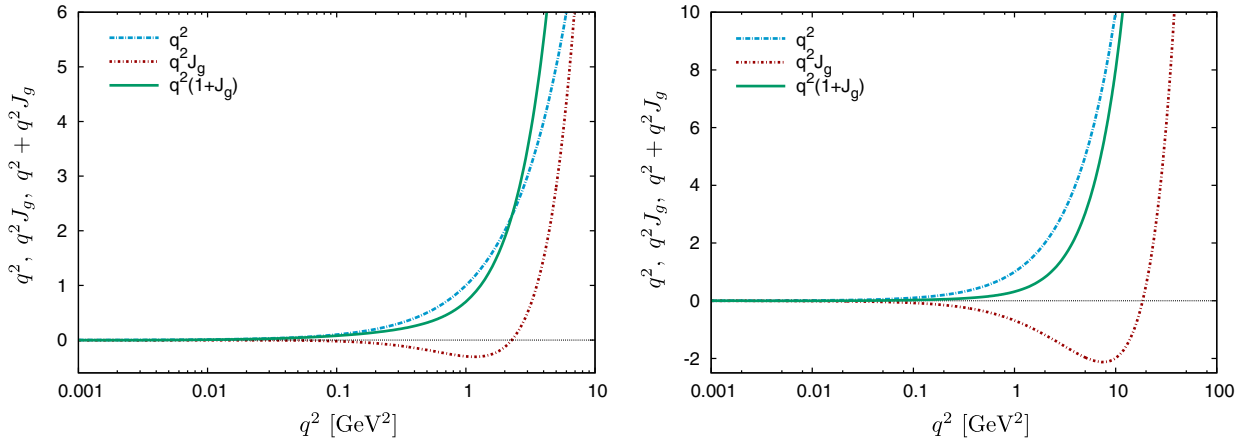

FIG. 9 (color online). Tree-level and quantum contributions to the gluon kinetic term for SU(2) (left panel) and SU(3) (right panel).

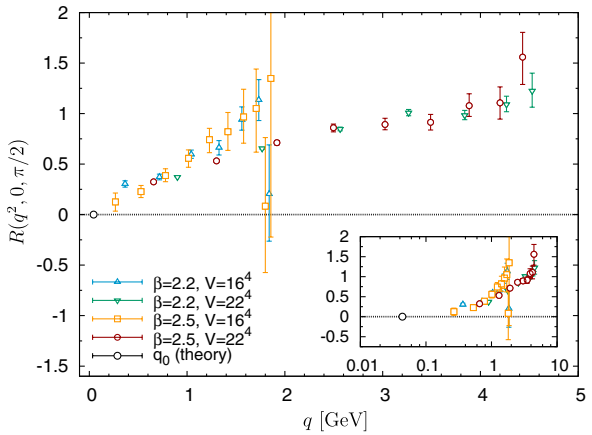

FIG. 10 (color online). Prediction for the zero crossing of the SU(2) form factor $R(q^2, 0, \pi/2)$ measured on the lattice in four dimensions [9]. The inset shows a logarithmic plot of the same quantity.

resolve them. Setting $k = 1$ (corresponding evidently to the minimum momentum which can be reached for a given L) and choosing the most coarse lattices used in the literature ($a \approx 21$ fm at $\beta = 2.5$ for the SU(2) case [9]), one obtains $L \sim 130$, which does not seem attainable with current simulations (which have $L = 22$ at most). In the SU(3) case, assuming that simulations can be performed at $\beta = 5.7$ with $a \approx 0.17$ fm (that is, in the same conditions used for simulating the gluon and ghost two-point sectors in Ref. [3]), one obtains instead $L \sim 60$. Obviously, these numbers are indicative, but they seem to suggest that resolving the zero crossing of R on the lattice in four dimensions could represent a challenging endeavor.

We next turn to the three-dimensional case. In the left panel of Fig. 11, we plot the full nonperturbative ghost kinetic term, evaluated using as input the functional fit to the $d = 3$ ghost dressing lattice data [2] given in Ref. [81].

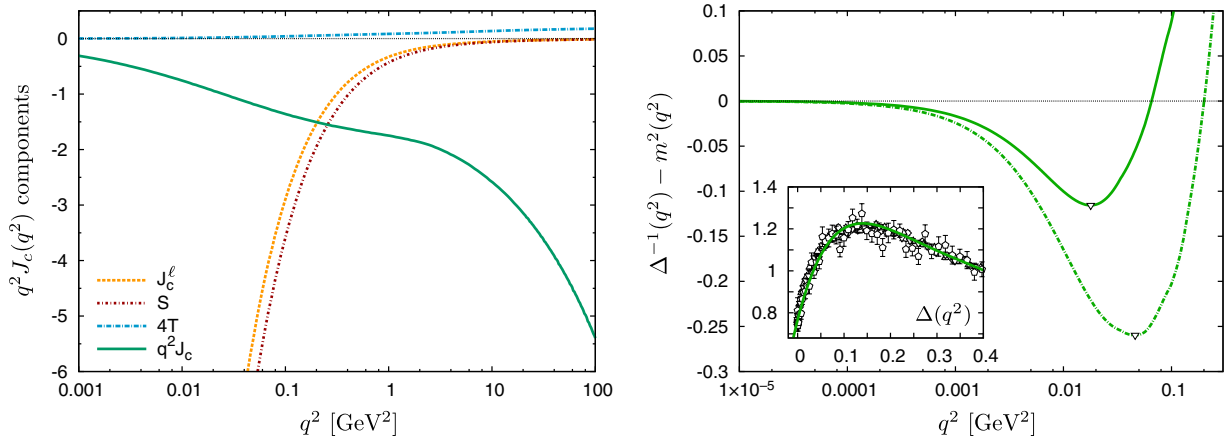

FIG. 11 (color online). The ghost kinetic term $q^2 J_c(q^2)$ (left panel) and the propagator's full kinetic part $\Delta^{-1}(q^2) - m^2(q^2)$ (right panel) for the SU(2) three dimensional case. The two curves in the right panel correspond to two different runnings for the dynamical mass. Finally, the inset in the same panel shows the IR propagator fit together with the corresponding lattice data of Ref. [2].

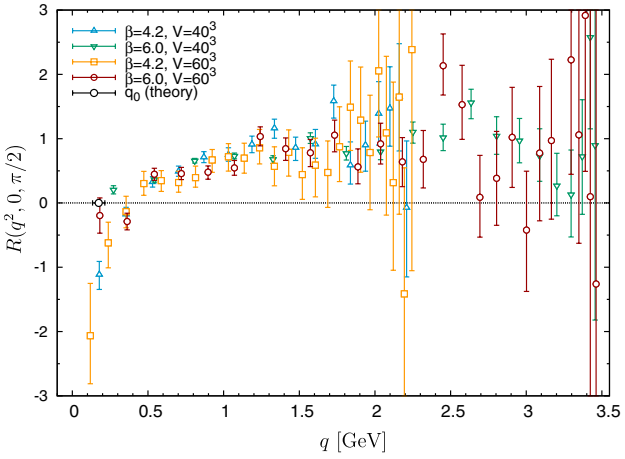

FIG. 12 (color online). Prediction for the zero-crossing of the SU(2) form factor $R(q^2, 0, \pi/2)$, measured on the lattice in three dimensions [9]. The point shown is the average of the minima of the kinetic term for the two different runnings of the dynamical mass, with the error corresponding to the semidifference of these two points.

One easily recognizes the expected linear divergence, which eventually translates into the well-known peak structure displayed in the IR by the gluon propagator (right panel inset) [2]. However, to repeat in $d = 3$, the exercise of obtaining the kinetic term $q^2J(q^2)$ from Eq. (3.28), an additional assumption is needed. Specifically, whereas the mass equation (3.23) is valid also in $d = 3$, the term Y has not been computed in this case; as a consequence, no solutions for $m^2(q^2)$ are available. We will circumvent this difficulty by simply *assuming* that the three-dimensional gluon mass behaves in a way similar to that of $d = 4$.

Given the need for this additional assumption, it is natural to consider the corresponding results for $q^2J(q^2)$ as less definite than in the $d = 4$ case. In fact, to acquire a quantitative notion of how the running of the mass influences these results, we carry out the analysis twice, once for the four-dimensional $m^2(q^2)$ obtained for SU(2) and once for the corresponding mass in SU(3). The results are shown in the right panel of Fig. 11. Depending on the mass solution used, the position of the minimum of the kinetic term is located between $q_0 \approx 134$ [SU(2) mass) and $q_0 \approx 215$ MeV (SU(3) mass]; this compares relatively well with lattice simulations of R (Fig. 12), which locate the zero crossing at around 380 MeV.

Let us finally point out that before the present work the appearance and location of the zero crossing has also been treated in Refs. [16] and [38], for $d = 3$ and $d = 4$, respectively, employing distinct approaches and approximations for the evaluation of the corresponding three-gluon vertices. In addition, very recent studies [82,83] appear to be in agreement with the general picture put forth here.

IV. CONCLUSIONS

In this work we have presented a set of connections that link the IR behavior of the gluon two- and three-point sector in quenched QCD. Specifically, we have shown that the fact that the ghost field remains nonperturbatively massless, as opposed to the gluon which acquires a dynamically generated mass, implies unavoidably the existence of a negative IR divergence in the dimensionless cofactor $J(q^2)$ of the kinetic part of the gluon propagator (in $d = 4$, $J \sim \ln q^2$, and in $d = 3$, $J \sim 1/q$). This divergence, originating exclusively from the one-loop dressed diagrams involving a ghost loop, does not affect the finiteness of the gluon two-point function, since the full kinetic term is multiplied by a q^2. However, its presence manifests itself in at least three different ways: first, the dimensionful kinetic part $q^2J(q^2)$ has a minimum, located at q_J; second, the full gluon propagator $\Delta(q^2)$ displays a maximum, at a point denoted by q_Δ; third, a (negative) divergence emerges in certain kinematic limits of the three-gluon sector, where the standard lattice projector, $R(q^2)$, is proportional to $J(q^2)$—the point where $R(q^2)$ vanishes is denoted by q_0.

The PT-BFM formalism turns out to be particularly suited for verifying the above picture quantitatively, mainly because it allows for a gauge-invariant separation of the ghost and gluon contributions to the gluon propagator. Consequently, one can identify the divergent ghost term in a meaningful and unambiguous way. Specifically, the fact that the special ghost-gluon vertex $\tilde{\Gamma}_\mu$ satisfies the QED-like WI of Eq. (3.9) furnishes a closed all-order expression for its longitudinal part, which is not possible to obtain for the corresponding vertex of the conventional (R_ξ) formulation. In addition, when one combines the aforementioned feature of individual transversality with the gluon mass equation and the available large-volume lattice data, one is able to separate gauge invariantly the gluon- and ghost-loop contributions to the full kinetic term $q^2J(q^2)$.

At the level of the SDE the IR-finite solutions (denominated as "decoupling" or "massive") have been obtained in two distinct ways. In the approach of Ref. [13], the Gribov horizon condition is appropriately implemented, and the resulting procedure signals a breaking of the global BRST symmetry. In the approach put forth in Ref. [12], the emergence of such solutions occurs through the introduction of massless poles in the corresponding vertices, following the standard Schwinger mechanism, and no BRST breaking has been identified, at least not at the level of the STIs satisfied by the massive Green's functions. The way confinement is realized within these two approaches is also quite distinct. Within the former scenario, it has been argued in Ref. [22] that the decoupling solutions satisfy a rather concrete confinement criterion derived from the effective action of the theory. Within the latter approach, the situation regarding confinement is considerably more involved, and no simple criterion has

been put forth to date. In particular, the dynamical gluon mass gives rise to a low energy effective theory, which supports a type of quantum solitons ("thick" center vortices), not present in the massless theory, for which the condensation furnishes an area law to the fundamental representation Wilson loop, thus confining quarks (for a detailed exposition, see Ref. [61], Chapter VII).

An important question in this context is whether the main conclusions of the present work may be affected by the truncation scheme employed or if they are, in a sense, "truncation independent." The main effect is controlled by the ghost loop, which, in the PT-BFM scheme has the transversality-preserving property mentioned throughout the text. Its divergence is a consequence of the masslessness of the ghost propagators, which seems to be a well-established fact in this field. In addition, the longitudinal part of the ghost-gluon vertex is completely fixed from the WI that it satisfies, and if one accepts the behavior of the transverse part assumed in Appendix B, then its omission will not affect the main result. Of course, if the transverse part did not obey this constraint, one could not entirely discard the possibility of a perfect cancellation between the contribution of the longitudinal and transverse parts of the ghost-gluon vertex; however, it would seem to require a tremendous degree of fine-tuning. The situation is more or less similar for the analysis of the three-gluon vertex, and the corresponding divergence and the associated zero crossing point. More prone to truncation dependence may be the secondary result of this work, namely, the form of the "gluonic" contribution, $J_g(q^2)$, which is indirectly determined, using the lattice data for the full gluon propagator and the form of the gluon mass obtained from the corresponding mass equation [see Eq. (3.29)]. As explained in the corresponding subsection, the kernel of this latter integral equation has undergone a drastic simplification, mainly due to our imperfect knowledge of the (conventional) full three-gluon vertex entering in it. Given the ongoing effort to better determine the structure of this vertex [83], we hope to be able to return to this issue in the near future.

An additional interesting result in this context is the inequality between the special points q_J and q_Δ, namely, $q_J < q_\Delta$, which constitutes a a clear and definite prediction of this particular approach based on the gluon mass generation. Specifically, the aforementioned relation is a direct result of Eq. (3.22), and in particular of the monotonically decreasing nature of the gluon mass $m^2(q^2)$, as obtained from the corresponding dynamical equation. This relation, in conjunction with the indirect determination of $q^2 J_g(q^2)$ may provide valuable guidance in the effort to obtain the entire kinetic term of the gluon propagator from a complete treatment of the corresponding SDE.

In the study of the R projector, we have used as reference the results obtained for the vertex with three incoming background fields (B^3). The main reason for this choice is the simplifications obtained due to the Abelian-like WI satisfied by the B^3 vertex. This property, in turn, eliminates all complications related to the ghost-gluon kernel, thus exposing the essence of the basic effect. For a very particular kinematic configuration, R is expressed solely in terms of the kinetic term of the B^2 propagator, a fact that imposes an exact coincidence between $q_{\hat{0}}$ and $q_{\hat{\jmath}}$.

Then, the corresponding results for the conventional vertex (Q^3) have been expressed as deviations from this prototypical case. Even though no exact results may be derived due to the "contamination" from the ghost-gluon vertex, the leading IR behavior can be accurately determined. On the other hand, the location of q_0 is not possible to pin down; however, it is reasonable to expect it to be relatively close to the corresponding point obtained for B^3. Actually, this value compares rather well with the lattice data in $d = 3$; unfortunately, a similar comparison in $d = 4$ is practically unattainable, since the corresponding lattice simulations have not as yet firmly evidenced a sign change in R.

In this respect, it should be noticed that, if taken at face value, our results predict that the lattice volumes required in order to observe this zero-crossing point are definitely large. This is a consequence of the fact that the divergence in J is only logarithmic in $d = 4$, something that pushes the zero crossing further into the IR, when compared to the $d = 3$ case (where the divergence in J is linear). Indeed, even if one assumes a factor of 2 inaccuracy in the determination of q_0, one would still need $L \sim 65$ (at $\beta = 2.5$ and $a \approx 21$ fm) for the SU(2) gauge group and $L \sim 30$ (at $\beta = 5.7$ and $a \approx 17$ fm) for SU(3). It would seem, therefore, that SU(3) lattice simulations would offer better prospects in identifying the divergence in the R projector.

Our analysis suggests that the sort of IR divergence considered here is likely to appear in other Green's functions that contain a ghost loop at lowest order in perturbation theory (Fig. 13). In fact, the four-gluon vertex [84–86], which constitutes one of the important missing ingredients in the various SDE studies [87], is a prime candidate for having such a divergence, due to the (one-loop) boxlike ghost diagram. On the other hand, a Green's function containing (at least) one external $\bar{c}c$ pair, (for example, the ghost-gluon vertex) cannot have such a graph at one loop; this type of graph appears at higher orders, and the additional loop integrations are expected to smooth out the original divergence. It would be interesting to test the above conjectures by means of detailed calculations.

Returning to the four-gluon vertex, on general grounds one would expect that the aforementioned divergence will manifest themselves at the level of individual diagrams, such as that shown in (Fig. 13). Of course, a simple perturbative calculation would give us the first indication of such a divergence; however, similar divergences will also come from the gluonic graphs, and the real effect might be

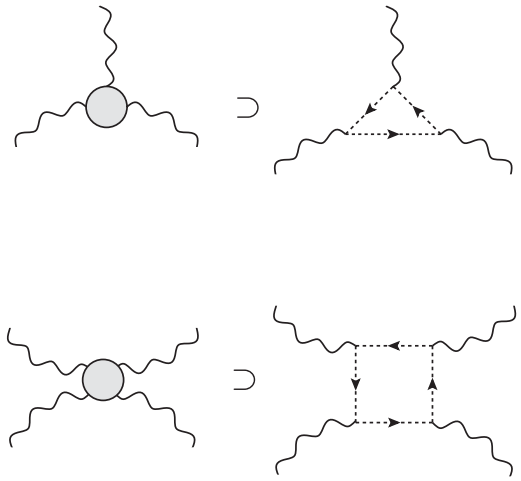

FIG. 13. The lowest order diagrams displaying a ghost loop in the case of the three- and four-gluon sector.

distorted, or hard to discern. Instead, it would seem more advantageous to introduce a nonperturbative (massive vs massless) distinction between gluons and ghosts, in the spirit of the present work. In this way, if there, the conjectured divergence of the ghost graphs will be cleanly exposed. This particular approach may be best implemented within the BT-BFM framework, given the unambiguous separation between gluonic and ghost contributions that it provides.

Since the origin of the effects described above is exclusively related to the presence of massless ghost loops, the act of "unquenching" is not expected to modify our results in a significant way. Indeed, large-volume lattice simulations [5] and the corresponding SDE analysis [88,89] have explicitly shown that even when dynamical quarks are present (i) the ghost remains massless and (ii) the gluon acquires dynamically a (heavier) mass. As a result, the machinery developed here is directly applicable to the unquenched case, with the minimal modification $\Delta_{\rm Q}^{-1}(q^2) - m_{\rm Q}^2(q^2) = q^2(J_c + J_g + J_q)$, where $\Delta_{\rm Q}^{-1}(q^2)$ and $m_{\rm Q}^2$ represent, respectively, the unquenched inverse propagator and dynamical mass, while $q^2 J_q$ is the (IR finite) quark loop evaluated in Ref. [88,89].

ACKNOWLEDGMENTS

The research of J. P. is supported by the Spanish MEYC under Grant No. FPA2011-23596. The work of A. C. A is supported by the National Council for Scientific and Technological Development—CNPq under Grant No. 306537/2012-5 and Project No. 473260/2012-3 and by São Paulo Research Foundation—FAPESP through Project No. 2012/15643-1. We thank Axel Maas for making his lattice data available to us.

APPENDIX A: VERTEX B^3 AND ITS R PROJECTOR

The B^3 vertex exposes the basic divergent features of the R projector, without the additional complications of the conventional vertex. In this Appendix we present some of the relevant technical points in this context.

At tree-level the B^3 and the conventional (Q^3) vertices coincide,

$$\begin{aligned}\hat{\Gamma}^{(0)}_{\alpha\mu\nu}(q,r,p) &= \Gamma^{(0)}_{\alpha\mu\nu}(q,r,p) \\ &= (q-r)_\nu g_{\alpha\mu} + (r-p)_\alpha g_{\mu\nu} + (p-q)_\mu g_{\alpha\nu},\end{aligned} \tag{A1}$$

where all momenta are entering. Beyond tree level the two vertices differ and are related by a complicated all-order BQI; in addition, both vertices are completely Bose symmetric.

More important in the present context is the fact that that $\hat{\Gamma}$ satisfies Abelian WIs; one has

$$q^\alpha \hat{\Gamma}_{\alpha\mu\nu}(q,r,p) = p^2 \hat{J}(p^2) P_{\mu\nu}(p) - r^2 \hat{J}(r^2) P_{\mu\nu}(r), \tag{A2}$$

with

$$J(q^2) = F^2(q^2)\hat{J}(q^2); \tag{A3}$$

cyclic permutations of indices and momenta generate the remaining WIs.

These identities are to be contrasted with the STIs satisfied by the conventional vertex

$$\begin{aligned}q^\alpha \Gamma_{\alpha\mu\nu}(q,r,p) = F(q^2)[&p^2 J(p^2) P^\alpha_\nu(p) H_{\alpha\mu}(p,q,r) \\ &- r^2 J(r^2) P^\alpha_\mu(r) H_{\alpha\nu}(r,q,p)],\end{aligned} \tag{A4}$$

(and cyclic permutations), which explicitly involve the ghost kernel H.

The complete closed form of $\hat{\Gamma}$ is not known; its longitudinal part, however, may be reconstructed by "solving" the identities (A2) [72]. Specifically, one begins by separating the vertex into the longitudinal and the (totally) transverse parts,

$$\hat{\Gamma}_{\alpha\mu\nu}(q,r,p) = \hat{\Gamma}^{\ell}_{\alpha\mu\nu}(q,r,p) + \hat{\Gamma}^{t}_{\alpha\mu\nu}(q,r,p), \tag{A5}$$

where the component $\hat{\Gamma}^{\ell}$ satisfies the WIs of Eq. (A2) (and its permutations), whereas $q^\alpha \hat{\Gamma}^t_{\alpha\mu\nu} = r^\mu \hat{\Gamma}^t_{\alpha\mu\nu} = p^\nu \hat{\Gamma}^t_{\alpha\mu\nu} = 0$.

The longitudinal part is then decomposed into 10 form factors, $\hat{X}_i$, according to

$$\hat{\Gamma}^{\ell}_{\alpha\mu\nu}(q,r,p) = \sum_{i=1}^{10} \hat{X}_i(q,r,p) \ell^i_{\alpha\mu\nu}, \tag{A6}$$

with the explicit form of the tensors ℓ^i given by [66]

$$\ell^1_{\alpha\mu\nu} = (q-r)_\nu g_{\alpha\mu}; \qquad \ell^2_{\alpha\mu\nu} = -p_\nu g_{\alpha\mu};$$
$$\ell^3_{\alpha\mu\nu} = (q-r)_\nu [q_\mu r_\alpha - (q\cdot r) g_{\alpha\mu}], \tag{A7}$$

with $\ell^{i+3}_{\alpha\mu\nu}$ given by cyclic permutations of momenta and indices and $\ell^{10}_{\alpha\mu\nu} = q_\nu r_\alpha p_\mu + q_\mu r_\nu p_\alpha$.

The WIs of Eq. (A2) give rise to an algebraic system for the $\hat{X}_i$, for which the solution reads [66]

$$\hat{X}_1 = \frac{1}{2}[\hat{J}(q^2) + \hat{J}(r^2)]; \qquad \hat{X}_2 = \frac{1}{2}[\hat{J}(q^2) - \hat{J}(r^2)];$$
$$\hat{X}_3 = \frac{\hat{J}(q^2) - \hat{J}(r^2)}{q^2 - r^2}, \tag{A8}$$

with $\hat{X}_{i+3}$ obtained from $\hat{X}_i$ as before and with $\hat{X}_{10} = 0$.

We thus see that the longitudinal form factors constituting $\hat{\Gamma}^\ell$ involve *only* the quantity $\hat{J}$; instead, as seen in Eqs. (3.33) and (3.34), the corresponding expressions for the form factors of the conventional vertex, contain, in addition, the ghost dressing function F and the various form factors comprising the gluon-ghost kernel H.

Finally, the (undetermined) transverse part of the vertex is described by four remaining form factors $\hat{Y}_i$,

$$\hat{\Gamma}^t_{\alpha\mu\nu}(q,r,p) = \sum_{i=1}^{4} \hat{Y}_i(q,r,p) t^i_{\alpha\mu\nu}, \tag{A9}$$

with the completely transverse tensors t^i given by

$$t^1_{\alpha\mu\nu} = [(q\cdot r) g_{\alpha\mu} - q_\mu r_\alpha][(r\cdot p) q_\nu - (q\cdot p) r_\nu], \tag{A10}$$

$t^2_{\alpha\mu\nu}$ and $t^3_{\alpha\mu\nu}$ obtained from this expression by cyclic permutations, and, finally,

$$t^4_{\alpha\mu\nu} = g_{\mu\nu}[(p\cdot q) r_\alpha - (r\cdot q) p_\alpha] + g_{\alpha\mu}[(r\cdot p) q_\nu - (q\cdot p) r_\nu] + g_{\alpha\nu}[(r\cdot q) p_\mu - (r\cdot p) q_\mu] + p_\alpha q_\mu r_\nu - r_\alpha p_\mu q_\nu. \tag{A11}$$

Using these decompositions, it is straightforward to evaluate the R projector defined in Eq. (3.30). In particular, one obtains (in d dimensions)[12] [77]

$$\mathcal{N}^\ell(q,r,p) = 4\frac{r^2p^2 - (r\cdot p)^2}{q^2r^2p^2}\{[(d-1)q^2r^2 - (q\cdot p)(p\cdot r)]\hat{A}_1 + [(d-1)r^2p^2 - (p\cdot q)(q\cdot r)]\hat{A}_2 + [(d-1)q^2p^2 - (q\cdot r)(r\cdot p)]\hat{A}_3 + [(q\cdot r)(r\cdot p)(p\cdot q) - q^2r^2p^2]\hat{A}_4\},$$
$$\mathcal{N}^t(q,r,p) = 2[r^2p^2 - (r\cdot p)^2]\{[(d-1)(q\cdot r) - p^2]\hat{Y}_1 + [(d-1)(r\cdot p) - q^2]\hat{Y}_2 + [(d-1)(q\cdot p) - r^2]\hat{Y}_3 + 3(d-2)\hat{Y}_4\} \tag{A12}$$

and

$$\mathcal{D}(q,r,p) = 4\frac{r^2p^2 - (r\cdot p)^2}{q^2r^2p^2} \times [(d-1)(q^2r^2 + q^2p^2 + r^2p^2) + (r\cdot p)^2 - r^2p^2], \tag{A13}$$

where we have defined $\mathcal{N} = \mathcal{N}^\ell + \mathcal{N}^t$, while the combinations $\hat{A}_i$ are given by

$$\hat{A}_1 = \hat{X}_1 - (q\cdot r)\hat{X}_3; \qquad \hat{A}_2 = \hat{X}_4 - (r\cdot p)\hat{X}_6;$$
$$\hat{A}_3 = \hat{X}_7 - (p\cdot q)\hat{X}_9; \qquad \hat{A}_4 = -\hat{X}_3 - \hat{X}_6 - \hat{X}_9. \tag{A14}$$

We next consider three particular kinematic configurations of the $\hat{R}$ projector, which are typically simulated on the lattice [8,9]. Interestingly enough, as we will see, they all display the same exact divergent behavior in the IR.

[12]Notice that the following expressions are general and apply also to the conventional vertex case, with the obvious replacements $\hat{X}_i \to X_i$, where the X_i are now determined by the STIs (A4).

1. Orthogonal configuration with one momentum vanishing

In this case we take $\varphi = \pi/2$ and $r \to 0$; as in the latter limit, $\mathcal{N}^t$ vanishes, and we obtain the simple result [77]

$$\hat{R}(q^2, 0, \pi/2) = [q^2\hat{J}(q^2)]'. \tag{A15}$$

The above result is exact, and valid for any q^2; in particular, using Eqs. (A3) and (3.19), we find the leading IR behavior to be

$$\hat{R}(q^2, 0, \pi/2) \underset{q^2\to 0}{=} C_d F^{-1}(0) \int_k \frac{F(k)}{k^2(k+q)^2}. \tag{A16}$$

If at this point we set $F = 1$, and carry out the resulting (effectively one-loop) integral, we recover Eq. (2.22).

It is interesting to observe that in this case, since Eq. (A15) is exact, $\hat{R}^{s\ell}$ vanishes identically, so that the condition Eq. (3.47) simplifies to

$$\hat{R}(\hat{q}^2_\Delta) = -[\hat{m}^2(\hat{q}^2_\Delta)]'. \tag{A17}$$

This means that for the equality $\hat{q}_\Delta = \hat{q}_0$ to hold, the mass $\hat{m}^2(q^2) = F^{-2}(q^2)m^2(q^2)$ should not be monotonic; while

a preliminary study shows that this is indeed what happens, this issue needs to be thoroughly investigated.

Note, finally, that the ratio between Eq. (3.46) and Eq. (A16) is finite and given by

$$\frac{R(0)}{\hat{R}(0)} = F^3(0), \tag{A18}$$

as was first derived in Ref. [77], following different considerations.

2. Orthogonal configuration with equal momenta

In this case one has

$$q^2 = r^2; \quad q\cdot r = 0; \quad p^2 = 2q^2;$$
$$q\cdot p = r\cdot p = -q^2; \quad \varphi = \pi/2. \tag{A19}$$

Clearly, in this configuration, the transverse part of the vertex survives,

$$\frac{\mathcal{N}^t(q^2,q^2,\pi/2)}{\mathcal{D}(q^2,q^2,\pi/2)} = \frac{q^2}{5d-6}[2q^2\hat{Y}_1 + dq^2(\hat{Y}_2+\hat{Y}_3) - 3(d-2)\hat{Y}_4], \tag{A20}$$

where $\hat{Y}_i = \hat{Y}_i(q^2,q^2,\pi/2)$. However, if we assume that the form factors $\hat{Y}_i$ do not contain poles in q^2, it is clear that this term vanishes in the IR. Then, from $\mathcal{N}^\ell$ we obtain

$$\hat{R}(q^2,q^2,\pi/2) = \frac{1}{5d-6}[2q^2\hat{J}'(q^2) - (d+4)\hat{J}(q^2) + 2(3d-1)\hat{J}(2q^2)] + \cdots, \tag{A21}$$

where the omitted terms are subleading in the IR. This result may be easily rearranged to read

$$\hat{R}(q^2,q^2,\pi/2) = \hat{J}(q^2) + \frac{1}{5d-6}\{2q^2\hat{J}'(q^2) + 2(3d-1)[\hat{J}(2q^2) - \hat{J}(q^2)]\}, \tag{A22}$$

where the first term is leading and coincides with that of Eq. (A16), while the second is subleading.

3. All momenta equal

Setting

$$q^2 = r^2 = p^2; \qquad q\cdot r = q\cdot p = p\cdot r = -\frac{q^2}{2};$$
$$\varphi = 2\pi/3, \tag{A23}$$

we find for the transverse part

$$\frac{\mathcal{N}^t(q^2,q^2,2\pi/3)}{\mathcal{D}(q^2,q^2,2\pi/3)} = \frac{q^2}{12d-15}[(d+1)q^2(\hat{Y}_1+\hat{Y}_2+\hat{Y}_3) - 6(d-2)\hat{Y}_4], \tag{A24}$$

where $\hat{Y}_i = \hat{Y}_i(q^2,q^2,2\pi/3)$. Again, this term may be neglected under the same assumptions stated above. Then, one finds

$$\hat{R}(q^2,q^2,2\pi/3) = \hat{J}(q^2) + \frac{2(d-1)}{4d-5}q^2\hat{J}'(q^2), \tag{A25}$$

thus obtaining exactly the same leading IR behavior as in the previous two cases.

APPENDIX B: TRANSVERSE PART OF THE VERTEX $\tilde{\Gamma}_\mu$

The contribution of the transverse part $\tilde{\Gamma}^t_\mu$ to $J_c(q^2)$, to be denoted by $J^t_c(q^2)$, is given, up to irrelevant constants and the finite ghost dressing function $F(q)$, by

$$q^2 J^t_c(q^2) \sim \int_k k^\mu D(k)D(k+q)\{(k\cdot q)(k+q)_\mu - [(k+q)\cdot q)]k_\mu\}\mathcal{A}(k,k+q) \sim \int_k D(k)D(k+q)\mathcal{A}(k,k+q)[(k\cdot q)^2 - q^2k^2]. \tag{B1}$$

So, after passing to spherical coordinates, and using that $(k\cdot q)^2 = q^2k^2\cos^2\theta$, we obtain

$$J^t_c(q^2) \sim \int_k D(k)D(k+q)\mathcal{A}(k,k+q)k^2\sin^2\theta. \tag{B2}$$

Now, at $q=0$, we have (setting $k^2 = y$)

$$J^t_c(0) \sim \int_k D^2(y)\mathcal{A}(y)y\sin^2\theta, \tag{B3}$$

with

$$\int_k = \frac{1}{(2\pi)^d}\frac{\pi^{\frac{d-1}{2}}}{\Gamma(\frac{d-1}{2})}\int_0^\pi d\theta\sin^{d-2}\theta\int_0^\infty dy y^{\frac{d}{2}-1}. \tag{B4}$$

The integration over the angle θ furnishes an additional irrelevant constant, and so, after using Eq. (2.2),

$$J^t_c(0) \sim \int_0^\infty dy y^{\frac{d}{2}-2}F^2(y)\mathcal{A}(y). \tag{B5}$$

Thus, if we assume that, in the deep IR, $\mathcal{A}(y)\sim y^a$, then the lower limit of this integral is finite provided that $a > 1 - d/2$ [remember that $F(y)$ saturates to a constant in the IR]. Thus, for $d=4$, one gets a finite (and,

therefore, subleading) contribution to $J_c(q^2)$, provided that $\mathcal{A}(y)$ diverges more weakly than a simple pole. In $d=3$, the corresponding limiting case is a square root of a pole.

To analyze the situation a bit further, let us concentrate on the $d=4$ case and consider the limiting case $a=-1$. It is interesting to observe that at the level of $\tilde{\Gamma}^t_\mu$ this does not necessarily correspond to a constant (nonvanishing) contribution in the IR. In particular, let us suppose that $\tilde{\Gamma}^t_\mu = [q_\mu(k\cdot q) - k_\mu q^2]/k^2$; then, if the limit $q\to 0$ is taken first, both components of $\tilde{\Gamma}^t_\mu$ vanish. However, since in order to isolate the contribution to $J^t_c(q^2)$ one has to factor out a q^2, the remainder will force $J^t_c(0)$ to diverge stronger than a logarithm.

In general terms, what one expects in this context is that $\mathcal{A}$ will not diverge, due to the infrared finiteness of the gluon propagator, which, in an effective way, acts as a mass scale in the diagrams defining $\tilde{\Gamma}_\mu$. Within this scenario, the additional scale that will saturate the dimensionality of $\tilde{\Gamma}^t_\mu$ will be related to some effective mass; in qualitative terms, one would expect a $\tilde{\Gamma}^t_\mu$ of the form $\tilde{\Gamma}^t_\mu = [q_\mu(k\cdot q) - k_\mu q^2]/(k^2+m^2)$, which would correspond to $a=0$. Of course, a more subtle interplay between momenta and masses may occur, giving rise to other values of the parameter a. However, a more concrete statement requires a detailed analysis that is beyond our present powers.

Let us finally point out that there is no known way that would permit one, at a practical level, to deduce the behavior of $\tilde{\Gamma}_\mu$ (or $\tilde{\Gamma}^t_\mu$) from the fact that the conventional ghost-gluon vertex, Γ_μ, reaches a finite value in the kinematic limit considered above. The main reason for this can be traced back to the exact, but rather complicated, relation between $\tilde{\Gamma}_\mu$ and Γ_μ, derived in Eq. (E.26) of Ref. [24]. This relation is a BQI, in the sense of Eq. (2.4), but, unlike Eq. (2.4), it receives additional contributions involving auxiliary fields and sources, characteristic of the Batalin–Vilkovisky formalism [90,91]. These latter terms have a definite diagrammatic vertexlike structure, but their contributions have not been worked out to date.

APPENDIX C: BFM GREEN'S FUNCTIONS: A PROMISING ALTERNATIVE

It is clear from the main analysis that the mildness of the ghost-loop divergence in $d=4$ makes the main effects rather difficult to discern. In the case of the gluon propagator, the available lattice data are at most indicative of the presence of the (expected) maximum, for which the existence and location has been essentially assumed (and then appropriately modelled). In fact, its general location happens to be in the region where statistical as well as systematic uncertainties are (currently) relatively large. A similar difficulty occurs with the zero crossing and the subsequent negative divergence in the R projector.

It would be clearly desirable to consider alternative quantities, which might better capture and expose the aforementioned effect. To that end, we propose that the BFM Green's functions could be better suited for this particular study. In particular, the direct simulation of these quantities would help one to unambiguously settle several related questions.

The hope that the BFM Green's function might furnish certain advantages in this context, is based on the study of the the gluon propagator, $\hat{\Delta}(q^2)$. The latter has a precise field theoretic defintion, corresponding to the correlator of two background gluons B, i.e., $\langle 0|T[B_\mu(0)B_\nu(x)]|0\rangle$.

The *expected* result of a *direct* simulation of this quantity may be obtained by means of the BQI (2.5) together with the approximation (2.6). The general idea is that $\hat{\Delta}(q^2)$ will be enhanced with respect to the conventional (Q^2) propagator $\Delta(q^2)$ by the function $F^2(q^2)$, which is quite sizable in the IR [remember, for $\mu = 4.3$ GeV, $F(0)=2.7$]. In the

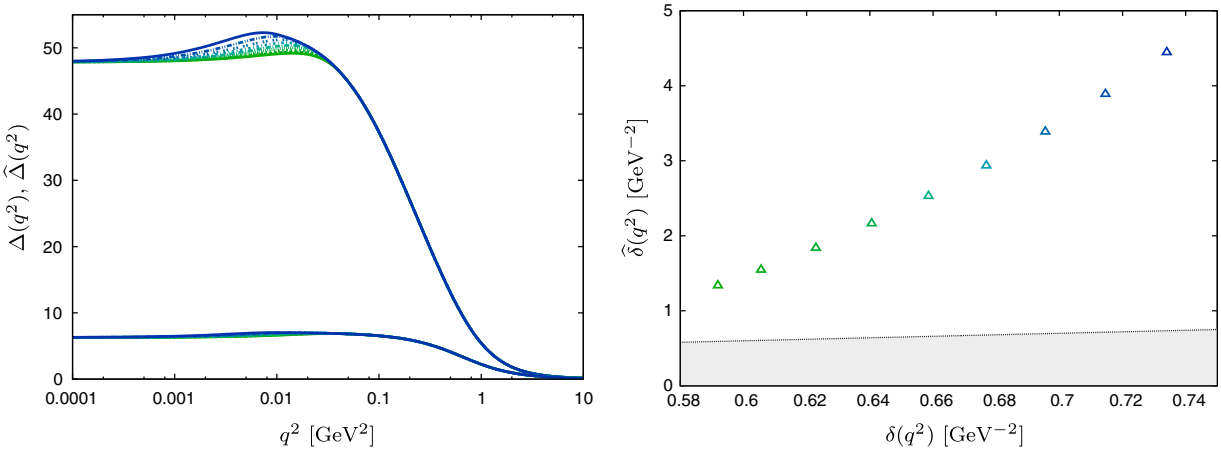

FIG. 14 (color online). Left panel: Comparison between the family of SU(3) propagators $\Delta(q^2)$ obtained in the numerical analysis of Sec. III E and the corresponding family $\hat{\Delta}(q^2)$ derived by applying the BQI (2.5); the color code is the same as in Fig. 6. Right panel: Sensitivity to the presence of an IR peak for the B^2 propagator ($\hat{\delta}$) vs the same quantity for the conventional propagator (δ). The shaded area corresponds to the region $\hat{\delta}\leq\delta$.

left panel of Fig. 14, we present the family of SU(3) propagators $\Delta(q^2)$ with variable (barely visible) maxima studied in Sec. III E and the corresponding family of $\hat{\Delta}(q^2)$, obtained from the application of Eq. (2.5). It is clear that the corresponding maxima of the resulting $\hat{\Delta}(q^2)$ are considerably easier to discern.

To be more quantitative, let us define the quantities

$$\delta(q^2_\Delta) = \Delta(q^2_\Delta) - \Delta(0); \qquad \hat{\delta}(q^2_{\hat{\Delta}}) = \hat{\Delta}(q^2_{\hat{\Delta}}) - \hat{\Delta}(0), \tag{C1}$$

which give a measure of the corresponding propagator's "sensitivity" to the presence of a peak in the IR [as δ ($\hat{\delta}$) increases the resolution of the maximum becomes easier]. Then, in the right panel of Fig. 14, we plot $\hat{\delta}$ vs δ; as one can clearly see, one has $\hat{\delta} > \delta$ and the enhancement factor in the sensitivity is between 2 and 7; the price one has to pay is a modest shift toward the IR of the peak location.

One may find analogous advantages in the case of the BFM three-point function, $\langle 0|T[B_\mu(0)B_\nu(x)B_\nu(y)]|0\rangle$ and the corresponding $\hat{R}$, considered in Appendix A. In particular, in this case the location of the zero crossing coincides exactly with that of the maximum of $\hat{\Delta}$, since there is no contamination from the ghost sector of the theory [e.g., the relation (A15) is exact]. This clearly furnishes a rather powerful test of the self-consistency of the entire approach.

Similarly, one may envisage the study of the corresponding four-point function, especially in view of the expectation that it displays divergences for some kinematic configurations. Thus, it might be worth considering a lattice quantity analogous to $\hat{R}$ for the case of the four-gluon vertex. Of course, a detailed study is required in order to identify the kinematic choices that will best expose the underlying divergence, be it in the form of a zero crossing or some other distinctive feature.

Let us finally point out that recently the procedure for fixing the minimal Landau background gauge within a nonperturbative lattice formulation has been identified in Ref. [92,93]; this development puts the prospects of lattice simulation of background quantities, such as those proposed here, on a much firmer theoretical ground.

APPENDIX D: COMPARISON WITH THE SCALING SOLUTIONS

It is well known that the coupled system of SDEs for the gluon and ghost propagators admits a particular solution displaying an IR behavior which is qualitatively different to those considered here. Specifically, this so-called "scaling solution" [17] exhibits a power-law IR behavior for both the gluon propagator as well as the ghost dressing function, with $\Delta \sim (q^2)^{2\kappa-1}$, $F \sim (q^2)^{-\kappa}$, and $\kappa \approx 0.595$. Therefore, one has an IR-suppressed gluon propagator, $\Delta(0) = 0$, and an enhanced ghost dressing function, since $F(0) \to \infty$.

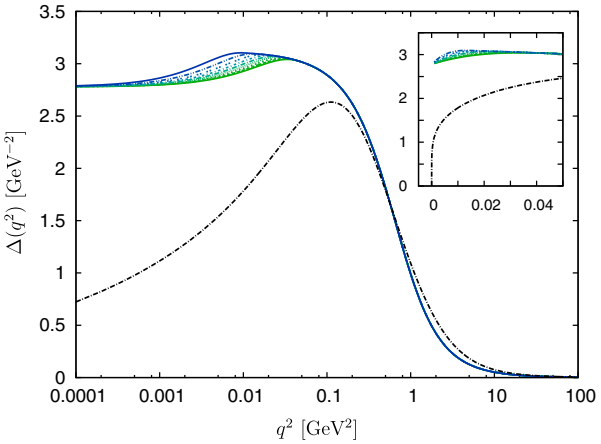

FIG. 15 (color online). Comparison between the Landau gauge propagators obtained through our analysis, and the so-called scaling solution [17] (black, dashed-dotted line). The inset represents a zoom on the deep IR region in the linear scale, which makes manifest that, in the scaling case, the gluon propagator vanishes.

According to our analysis, such an enhanced ghost sector would imply a power-law divergent ghost loop, even in the $d = 4$ case (similar to what happens for the $d = 3$ "massive" case). As a consequence, the scaling gluon propagator is expected to show a well-resolved peak structure, with a maximum located at a relatively large momentum value.

The precise comparison shown in Fig. 15 confirms this expectation. Specifically, in Fig. 15 we contrast the set of massive (decoupling) SU(3) propagators used in our analysis (shown in Fig. 6) with the set of data corresponding to the scaling solution of Ref. [17]; to ease the comparison, all propagators have been normalized such that they match in the UV. For the scaling solution, one finds $q_\Delta \approx 330$ MeV, to be compared with the average value $q_\Delta \sim 100$ MeV for the massive case. The enhanced ghost sector, together with the associated shift in the propagator peak, should then suffice to explain the somewhat higher results quoted in Ref. [83] for the zero-crossing location q_0.

[1] A. Cucchieri and T. Mendes, *Proc. Sci.*, LAT2007 (**2007**) 297.
[2] A. Cucchieri and T. Mendes, *Proc. Sci.*, QCD-TNT09 (**2009**) 026.
[3] I. Bogolubsky, E. Ilgenfritz, M. Muller-Preussker, and A. Sternbeck, Phys. Lett. B **676**, 69 (2009).
[4] O. Oliveira and P. Silva, *Proc. Sci.*, LAT2009 (**2009**) 226.
[5] A. Ayala, A. Bashir, D. Binosi, M. Cristoforetti, and J. Rodriguez-Quintero, Phys. Rev. D **86**, 074512 (2012).
[6] A. Sternbeck, L. von Smekal, D. Leinweber, and A. Williams, *Proc. Sci.*, LAT2007 (**2007**) 340.
[7] P. O. Bowman, U. Heller, D. Leinweber, M. Parappilly, A. Sternbeck, L. von Smekal, A. Williams, and J. Zhang, Phys. Rev. D **76**, 094505 (2007).
[8] A. Cucchieri, A. Maas, and T. Mendes, Phys. Rev. D **74**, 014503 (2006).
[9] A. Cucchieri, A. Maas, and T. Mendes, Phys. Rev. D **77**, 094510 (2008).
[10] E.-M. Ilgenfritz, M. Muller-Preussker, A. Sternbeck, A. Schiller, and I. Bogolubsky, Braz. J. Phys. **37**, 193 (2007).
[11] P. Boucaud, J. P. Leroy, A. Le Yaouanc, J. Micheli, O. Pène, and J. Rodríguez-Quintero, J. High Energy Phys. 06 (2008) 099.
[12] A. Aguilar, D. Binosi, and J. Papavassiliou, Phys. Rev. D **78**, 025010 (2008).
[13] C. S. Fischer, A. Maas, and J. M. Pawlowski, Ann. Phys. (Amsterdam) **324**, 2408 (2009).
[14] J. Rodriguez-Quintero, J. High Energy Phys. 01 (2011) 105.
[15] M. Pennington and D. Wilson, Phys. Rev. D **84**, 119901 (2011).
[16] D. R. Campagnari and H. Reinhardt, Phys. Rev. D **82**, 105021 (2010).
[17] R. Alkofer and L. von Smekal, Phys. Rep. **353**, 281 (2001).
[18] P. Maris and C. D. Roberts, Int. J. Mod. Phys. E **12**, 297 (2003).
[19] A. C. Aguilar and A. A. Natale, J. High Energy Phys. 08 (2004) 057.
[20] C. S. Fischer, J. Phys. G **32**, R253 (2006).
[21] K.-I. Kondo, Phys. Rev. D **74**, 125003 (2006).
[22] J. Braun, H. Gies, and J. M. Pawlowski, Phys. Lett. B **684**, 262 (2010).
[23] D. Binosi and J. Papavassiliou, Phys. Rev. D **77**, 061702 (2008).
[24] D. Binosi and J. Papavassiliou, J. High Energy Phys. 11 (2008) 063.
[25] K.-I. Kondo, Phys. Rev. D **84**, 061702 (2011).
[26] A. P. Szczepaniak and E. S. Swanson, Phys. Rev. D **65**, 025012 (2001).
[27] A. P. Szczepaniak, Phys. Rev. D **69**, 074031 (2004).
[28] D. Epple, H. Reinhardt, W. Schleifenbaum, and A. Szczepaniak, Phys. Rev. D **77**, 085007 (2008).
[29] A. P. Szczepaniak and H. H. Matevosyan, Phys. Rev. D **81**, 094007 (2010).
[30] P. Watson and H. Reinhardt, Phys. Rev. D **82**, 125010 (2010).
[31] P. Watson and H. Reinhardt, Phys. Rev. D **85**, 025014 (2012).
[32] J. M. Cornwall, Phys. Rev. D **26**, 1453 (1982).
[33] C. W. Bernard, Nucl. Phys. **B219**, 341 (1983).
[34] J. F. Donoghue, Phys. Rev. D **29**, 2559 (1984).
[35] O. Philipsen, Nucl. Phys. **B628**, 167 (2002).
[36] A. Aguilar, D. Binosi, and J. Papavassiliou, Phys. Rev. D **84**, 085026 (2011).
[37] D. Binosi, D. Ibanez, and J. Papavassiliou, Phys. Rev. D **86**, 085033 (2012).
[38] M. Q. Huber and L. von Smekal, J. High Energy Phys. 04 (2013) 149.
[39] M. Pelaez, M. Tissier, and N. Wschebor, Phys. Rev. D **88**, 125003 (2013).
[40] A. Aguilar, D. Binosi, and J. Papavassiliou, Phys. Rev. D **81**, 125025 (2010).
[41] W. Schleifenbaum, M. Leder, and H. Reinhardt, Phys. Rev. D **73**, 125019 (2006).
[42] M. Q. Huber, R. Alkofer, C. S. Fischer, and K. Schwenzer, Phys. Lett. B **659**, 434 (2008).
[43] Y. Nakagawa, A. Voigt, E.-M. Ilgenfritz, M. Müller-Preussker, A. Nakamura, T. Saito, A. Sternbeck, and H. Toki, Phys. Rev. D **79**, 114504 (2009).
[44] J. M. Cornwall and J. Papavassiliou, Phys. Rev. D **40**, 3474 (1989).
[45] D. Binosi and J. Papavassiliou, Phys. Rev. D **66**, 111901(R) (2002).
[46] D. Binosi and J. Papavassiliou, J. Phys. G **30**, 203 (2004).
[47] D. Binosi and J. Papavassiliou, Phys. Rep. **479**, 1 (2009).
[48] L. F. Abbott, Nucl. Phys. **B185**, 189 (1981).
[49] A. C. Aguilar and J. Papavassiliou, J. High Energy Phys. 12 (2006) 012.
[50] P. A. Grassi, T. Hurth, and M. Steinhauser, Ann. Phys. (N.Y.) **288**, 197 (2001).
[51] D. Binosi and J. Papavassiliou, Phys. Rev. D **66**, 025024 (2002).
[52] A. Aguilar, D. Binosi, and J. Papavassiliou, J. High Energy Phys. 11 (2009) 066.
[53] P. A. Grassi, T. Hurth, and A. Quadri, Phys. Rev. D **70**, 105014 (2004).
[54] A. Aguilar, D. Binosi, J. Papavassiliou, and J. Rodriguez-Quintero, Phys. Rev. D **80**, 085018 (2009).
[55] A. Aguilar, D. Binosi, and J. Papavassiliou, J. High Energy Phys. 07 (2010) 002.
[56] P. Pascual and R. Tarrach, Lect. Notes Phys. **194**, 1 (1984).
[57] G. Alexanian and V. P. Nair, Phys. Lett. B **352**, 435 (1995).
[58] W. Buchmuller and O. Philipsen, Phys. Lett. B **397**, 112 (1997).
[59] F. Eberlein, Phys. Lett. B **439**, 130 (1998).
[60] D. Karabali, C.-j. Kim, and V. Nair, Phys. Lett. B **434**, 103 (1998).
[61] J. M. Cornwall, J. Papavassiliou, and D. Binosi, *The Pinch Technique and Its Applications to Non-Abelian Gauge Theories*, Cambridge Monographs on Particle Physics, Nuclear Physics, and Cosmology, Vol. 31 (Cambridge University Press, Cambridge, England, 2011).
[62] F. Karsch, T. Neuhaus, A. Patkos, and J. Rank, Nucl. Phys. **B474**, 217 (1996).
[63] A. Cucchieri, F. Karsch, and P. Petreczky, Phys. Rev. D **64**, 036001 (2001).
[64] U. M. Heller, F. Karsch, and J. Rank, Phys. Rev. D **57**, 1438 (1998).
[65] A. Nakamura, T. Saito, and S. Sakai, Phys. Rev. D **69**, 014506 (2004).

[66] M. Binger and S. J. Brodsky, Phys. Rev. D **74**, 054016 (2006).
[67] N. Ahmadiniaz and C. Schubert, Nucl. Phys. **B869**, 417 (2013).
[68] A. Cucchieri, T. Mendes, and A. R. Taurines, Phys. Rev. D **67**, 091502 (2003).
[69] C. D. Roberts and A. G. Williams, Prog. Part. Nucl. Phys. **33**, 477 (1994).
[70] D. C. Curtis and M. R. Pennington, Phys. Rev. D **42**, 4165 (1990).
[71] A. Kizilersu and M. Pennington, Phys. Rev. D **79**, 125020 (2009).
[72] J. S. Ball and T.-W. Chiu, Phys. Rev. D **22**, 2550 (1980).
[73] G. Eichmann and C. S. Fischer, Phys. Rev. D **87**, 036006 (2013).
[74] A. C. Aguilar and J. Papavassiliou, Phys. Rev. D **81**, 034003 (2010).
[75] P. Boucaud, F. De Soto, J. Leroy, A. Le Yaouanc, J. Micheli, O. Pène, and J. Rodríguez-Quintero, Phys. Rev. D **79**, 014508 (2009).
[76] B. Holdom, Phys. Lett. B **728**, 467 (2014).
[77] D. Binosi, D. Ibanez, and J. Papavassiliou, Phys. Rev. D **87**, 125026 (2013).
[78] D. Binosi and J. Papavassiliou, J. High Energy Phys. 03 (2011) 121.
[79] D. Ibañez and J. Papavassiliou, Phys. Rev. D **87**, 034008 (2013).
[80] H. Rothe, Lect. Notes Phys. **43**, 1 (1992).
[81] A. Aguilar, D. Binosi, and J. Papavassiliou, J. High Energy Phys. 01 (2012) 050.
[82] A. Blum, M. Q. Huber, M. Mitter, and L. von Smekal, arXiv:1401.0713.
[83] G. Eichmann, R. Williams, R. Alkofer, and M. Vujinovic, arXiv:1402.1365.
[84] P. Pascual and R. Tarrach, Nucl. Phys. **B174**, 123 (1980).
[85] J. Papavassiliou, Phys. Rev. D **47**, 4728 (1993).
[86] N. Ahmadiniaz and C. Schubert, arXiv:1311.6829.
[87] V. Mader and R. Alkofer, *Proc. Sci.*, ConfinementX (**2012**) 063.
[88] A. Aguilar, D. Binosi, and J. Papavassiliou, Phys. Rev. D **86**, 014032 (2012).
[89] A. Aguilar, D. Binosi, and J. Papavassiliou, Phys. Rev. D **88**, 074010 (2013).
[90] I. A. Batalin and G. A. Vilkovisky, Phys. Lett. **69B**, 309 (1977).
[91] I. A. Batalin and G. A. Vilkovisky, Phys. Rev. D **28**, 2567 (1983).
[92] D. Binosi and A. Quadri, Phys. Rev. D **85**, 121702 (2012).
[93] A. Cucchieri and T. Mendes, Phys. Rev. D **86**, 071503 (2012).